The Dissertation Committee for Dong-Hun Chae Certifies that this is the approved version of the following dissertation:

Electron Transport in Single-Molecule Transistors

Committee:

Zhen Yao, Supervisor

Allan H. MacDonald

Chih-Kang Ken Shih

Alejandro de Lozanne

Li Shi

Electron Transport in Single-Molecule Transistors

by

Dong-Hun Chae, B.A.; M.S.

Dissertation

Presented to the Faculty of the Graduate School of

The University of Texas at Austin

in Partial Fulfillment

of the Requirements

for the Degree of

Doctor of Philosophy

The University of Texas at Austin

August, 2006

This dissertation is dedicated to my father, HongBaek Chae

and my mother, BongAe Kim

Acknowledgements

I believe that my Ph.D. work has never been realized without others' help and encouragement for the past six years in Austin, Texas. I would like to acknowledge many people, whom I have met in my Ph.D. journey in Austin. Most of all, I would like to appreciate my advisor Prof. Zhen Yao. I thank him for giving me a chance to see and experience how experimental work can be realized from a *real* scratch. I am also indebted to him for his detailed instruction in the transport experiment as well as continuous discussion on the progress. His advice and guidance have been a driving force to continue my Ph.D. research. I would like to thank Prof. Alex de Lozanne, who generously allowed me to use facilities in his laboratory. I wish to thank Prof. Allan H. MacDonald, Prof. Ken Shih, and Prof. Li Shi for serving on my committee.

I am indebted to many collaborators related to my Ph.D. work. They are: Kang Luo, Suyong Jung in our group, Prof. Saiful I. Khondarker (former group member, now University of Central Florida), Dr. John F. Berry (Texas A&M University), Prof. F. Albert Cotton (Texas A&M University), Dr. Jeong Tae Lee (UT at Austin), Prof. Jonathan L. Sessler (UT at Austin), Prof. Alan Campion (UT at Austin), Dr. Qian Gu (Harvard University), Dr. Jens Koch (Freie Universität Berlin), Prof. Maxim Tsoi (UT at Austin) and Prof. Paul F. Barbara (UT at Austin).

I would like to express gratitude to the following people. They are: Allan Schroeder, Jack Clifford in the machine shop, Ed Baez, Lanny Sandefur in the cryoshop, Mike Tinner in Center for Nano and Molecular Science and Technology.

Many other colleagues and friends have also widened my understanding of physics during my staying in Austin. They are: Yunpil Shim, Dimi Culcer, Alvaro Nunez, Daejin Eom, DooYoung Kim, Hongki Min, Changbae Hyun, Joonho Bae, Byung-ick Cho, and Yong J Lee.

A special thank for useful comments on my thesis draft goes to Brian O'Gorman, Jason Hill and Dr. YoungJong Lee.

Finally, I wish to thank my parents and my sisters for encouraging me all the way through in my life.

Electron Transport in Single-Molecule Transistors

Publication No._____

Dong-Hun Chae, Ph.D.

The University of Texas at Austin, 2006

Supervisor: Zhen Yao

Electron transport through single molecules is greatly affected by electron-electron interactions, coupling between electron and internal vibrational modes, and the spin degree of freedom. In this thesis, we investigate electron transport in single-molecule transistors incorporating various molecules including trimetal complexes, porphyrins, and expanded porphyrins.

A strong coupling of tunneling electron to internal vibrational modes in single-molecule transistors (SMTs) distinguishes the transport characteristics from other single-electron transistors even though SMTs exhibit the single-electron tunneling behaviors due to the Coulomb interaction. In SMTs incorporating trimetal compounds, we have consistently observed low-energy excitations, which are most likely attributed to the internal vibrational modes. Interestingly, we have observed a dramatic change of these low-energy excitations with respect to electron charge state. In porphyrin-SMTs, we have found experimental evidences that higher-order tunneling occur via vibrationally excited states.

Electron transport through molecules is also significantly influenced by the spin degree of freedom through the Kondo effect. Conventional spin ½ Kondo effect has been reproducibly observed in single Co-porphyrin transistors. Interestingly, the Kondo effect is observed even in devices with very low conductance, which is distinct from earlier results. Furthermore, we have observed the absence of odd-even parity effect in the Kondo resonance in devices containing expanded porphyrins. Our observation can be understood if the exchange interaction within expanded porphyrin is strong enough to allow the net spin larger than ½ with even number of electrons similar to Hund's rule.

Finally, we describe progress of ongoing projects on the spin-dependent transport in the Coulomb interaction regime including the Kondo effect in the presence of ferromagnetism and magnetoresistance in SWNT devices.

Table of Contents

List of Figures

Chapter 1. Introduction

1.1 BACKGROUND

"Warning! Do not place this computer on your lap." is a caution comment of a label on your brand-new *laptop* computer. This contradictory situation shows that the modern electronic technology is confronting some problems. The transistor was invented by Shockley, Bardeen, and Brattain in 1947 (Nobel prize in 1956). Since the 1970's, silicon-based electronic devices have been continuously miniaturized. The large-scale integration of electronic circuits results in a state-of-art microprocessor containing more than 200 million transistors. The miniaturization is achieved using a photolithographic technology followed by etching techniques to create tiny structures from bulk Si wafers in the top-down approach.

The top-down approach, however is already confronting some physical limitations. Heat dissipation in integrated circuits is indeed serious as shown in the laptop example. The brutal force using a fan is not the right way to solve this heat problem. In addition, it is obvious that the operational mechanism of microdevices based on classical physics may not work well if the device dimension approaches some characteristic length scales such as the electron wavelength. Quantum mechanical effects set a fundamental barrier to the present operational mechanism of the devices.

Researchers are now looking for ways to change the present paradigm of technology. For instance, the spin-based electronics, so called spintronics[1] has been an active research area for the past few decades to utilize the quantum mechanical spin degree of freedom in order to improve the computing speed and to reduce the power consumption. Another attempt is the bottom-up approach, in which a nanoscale device is fabricated with nanotubes, nanowires, and even molecules as building blocks. In 1974,

Aviram and Ratner proposed an idea that single molecules can be utilized as a functional element in electronic switch[2, 3]. However, their proposal remained unrealized until the advance of science and technology enables true molecular scale structure. Several preliminary experimental demonstrations have been done in the laboratory. However, it is still a long way to achieve molecular electronics by assembling molecules into circuits in a technological sense at this moment.

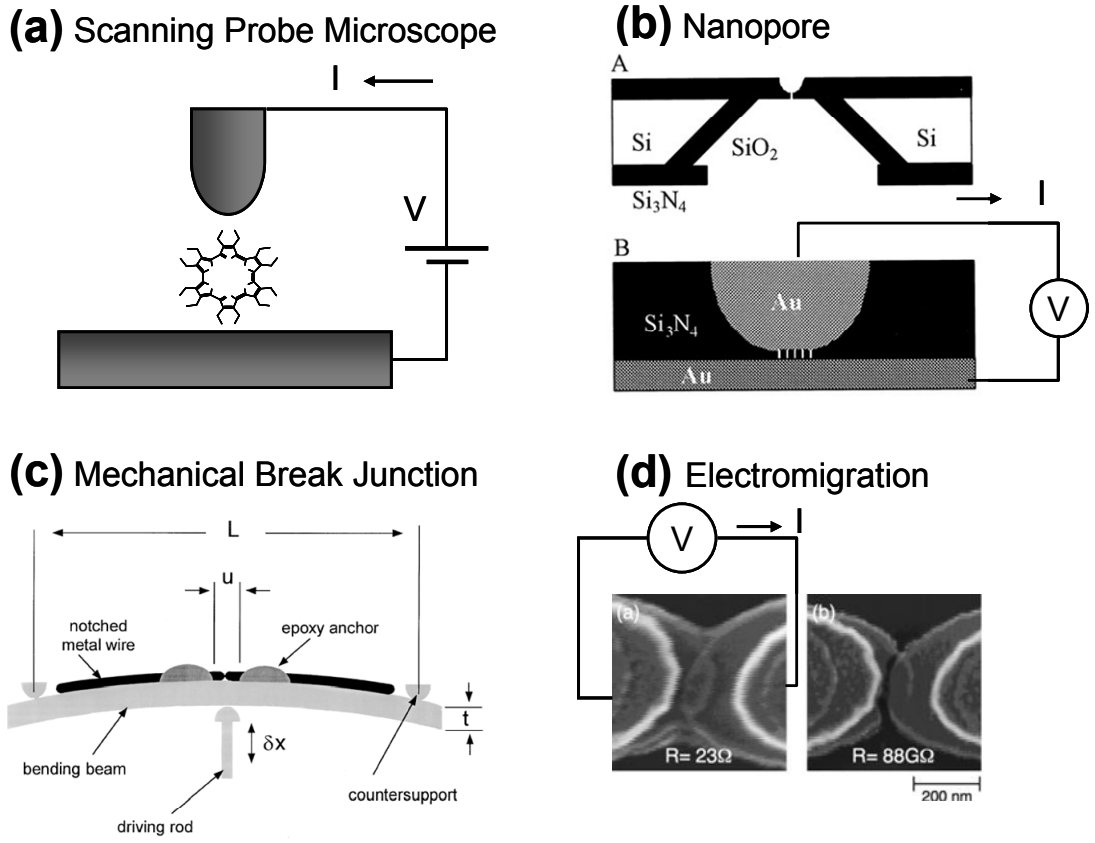

Figure 1.1 Various approaches to molecule studies. (a) Scanning probe technique. (b) Nanopore technique (from Ref. 4). (c) Mechanical break junction (from Ref. 5). (d) Electromigration (from Ref. 6).

1.2 PREVIOUS APPROACHES TO MOLECULE STUDIES

Researchers have tried to wire up individual molecules in several different ways even though those demonstrations are still for scientific interests and not application purposes.

First, scanning probe microscopy is applied to study molecules at the single molecule level as illustrated in Fig. 1.1 (a)[7-12]. An advantage of this technique is that the electronic transport properties can be investigated through a molecule unambiguously while "seeing" the molecule. However, it is a relatively challenging technique because the technique requires ultra high vacuum and cryogenic temperature. Nevertheless, many intriguing transport phenomena have been observed.

Second, researchers also developed a very small hole (<10 nm) in a silicon nitride membrane[4, 13, 14]. Electrical properties are investigated through molecules sandwiched between the upper and lower electrodes (Fig. 1.1 (b)). This technique enables the fabrication of many devices at the same time because the microfabrication process is applied. However, it is hard to measure molecules at the single molecule level since the hole size is relatively big compared to individual molecules.

Third, the mechanical break junction technique has been adopted to study a simple molecule such as H_2[15-18]. By bending the substrate, on which a metallic strip is fabricated, the metal strip is pulled and broken into two pieces. This leads to the exposure of two clean contacts (Fig. 1.1 (c)) and these clean surfaces are utilized to make contacts between a molecule and the leads. An advantage of this technique is that the gap size is easily tunable. However, the temperature dependent transport studies cannot be easily carried out because the gap size changes due to the thermal expansion of macroscopic mechanical parts.

All the above three techniques are basically a two-terminal technique. Therefore, the chemical potential and the charge states of molecule cannot be manipulated. Since the electronic states of the molecules are strongly influenced by local environment of the molecules, the spectroscopic information taken by the simple current-voltage measurement is limited. For instance, a nearby gate coupled to a molecule can overcome this situation. Recently, the electromigration technique[6] has been developed which enables the implementation of a gate to modify the electronic properties of the inserted molecules (Fig. 1.1 (d)). A metallic nanowire having a narrow constriction is fabricated by electron-beam lithography. The constriction is then broken like a simple fuse, but in quantized conductance by precisely ramping up an applied bias voltage at low temperature. It gives rise to a small gap corresponding to the size of molecules. Since H. Park and his collaborators demonstrated this technique with C_{60}[19], extensive work[20-27] has been followed by many other groups including us.

1.3 GENERIC CHARACTERISTICS OF TRANSPORT THROUGH INDIVIDUAL MOLECULES

A single-molecule transistor consists of a molecule connected by tunnel barriers to source and drain electrodes and a capacitively coupled gate (Fig. 1.2). The single molecule transistors that have been studied so far have all shown single-electron tunneling characterization at low temperature. The number of electrons in the molecule is a well-defined integer number, N, that can be controlled by varying the gate voltage like in a quantum dot. Tunneling of electron is blocked in the low bias regime due to repulsive Coulomb interaction until enough energy is provided by increasing the bias voltage across the source and drain electrodes. This phenomenon is known as the Coulomb blockade effect[28, 29]. This blockade can also be lifted by adjusting the induced

charge in the molecule by the gate such that the electrostatic energy of system is degenerate for N and N+1 charge states.

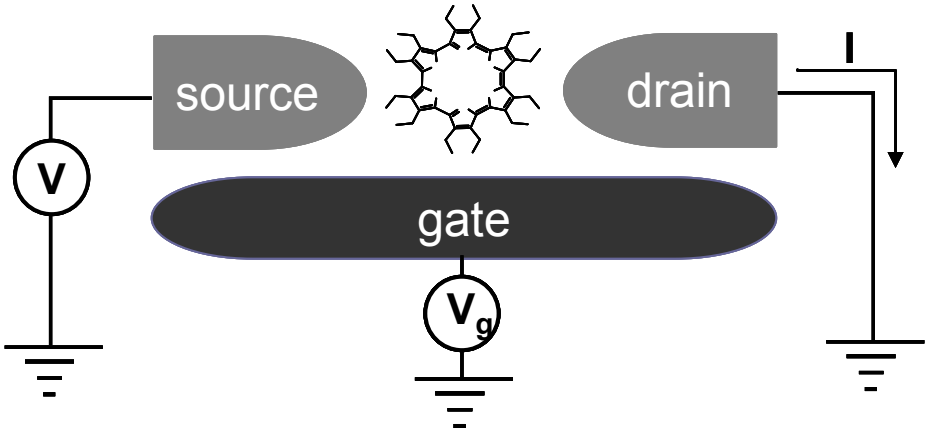

Figure 1.2 Schematic diagram of a single-molecule transistor.

One of the distinct characteristics in single molecule devices is that the tunneling electron is strongly coupled to the internal vibrational excitations of molecule because the vibrational relaxation time is quite long compared to the tunneling time of the electron. Consequently, higher-order inelastic tunneling processes typically arise through the vibrational excitations in molecules whereas the higher-order tunneling processes occur via electronic states in the semiconducting quantum dots[30].

The spin degree of freedom also greatly affects the transport characteristics in single molecule devices like in a quantum dot through the Kondo effect. The entanglement between a localized spin and conduction electrons in the leads by the exchange interaction results in an enhancement of conductance at zero bias voltage known as the Kondo resonance[31]. It turns out that a characteristics temperature as a

measure of the exchange interaction, the Kondo temperature can reach up to one hundred Kelvin in single-molecule transistors.

1.4 OUTLINE OF THE THESIS

This thesis is organized as follows: basic ideas including the Coulomb blockade effect, the cotunneling, and the Kondo effect are introduced in Chapter 2. In Chapter 3, experimental details are described including sample preparation and measurement setups. Chapter 4 presents experimental observations of vibrational excitations in single-molecule transistors incorporating trimetal molecules. In particular, a change of low-energy excitations is observed with respect to the charged (redox) state. Chapter 5 presents experimental results taken from porphyrin molecules. First, cotunneling features are shown within the Coulomb blockade zone. Second, prototypical spin ½ Kondo effects are consistently observed in Co-porphyrin transistors. Chapter 6 presents the observation that the Kondo resonance peaks appear regardless of the parity of the electron number in expanded porphyrin devices. This absence of the odd-even parity is interpreted qualitatively in the spirit of Hund's rule as in the atomic and molecular physics. Chapter 7 describes the motivations and progresses of ongoing projects on spin-dependent transport experiments in single molecule devices.

REFERENCES

[1] S. A. Wolf, D. D. Awschalom, R. A. Buhrman, J. M. Daughton, S. von Molnar, M. L. Roukes, A. Y. Chtchelkanova, and D. M. Treger, Science **294**, 1488 (2001).

[2] A. Aviram and M. A. Ratner, Chem. Phys. Lett. **29**, 277 (1974).

[3] A. Nitzan and M. A. Ratner, Science **300**, 1384 (2003).

[4] J. Chen, M. A. Reed, A. M. Rawlett, and J. M. Tour, Science **286**, 1550 (1999).

[5] J. M. van Ruitenbeek, A. Alvarez, I. Pineyro, C. Grahmann, P. Joyez, M. H. Devoret, D. Esteve, and C. Urbina, Rev. Sci. Instr. **67**, 108 (1996).

[6] H. Park, A. K. L. Lim, A. P. Alivisatos, J. Park, and P. L. McEuen, Appl. Phys. Lett. **75**, 301 (1999).

[7] C. Joachim, J. K. Gimzewski, R. R. Schlittler, and C. Chavy, Phys. Rev. Lett. **74**, 2102 (1995).

[8] B. C. Stipe, M. A. Rezaei, and W. Ho, Science **280**, 1732 (1998).

[9] D. Porath, Y. Levi, M. Tarabiah, and O. Millo, Phys. Rev. B **56**, 9829 (1997).

[10] X. D. Cui, A. Primak, X. Zarate, J. Tomfohr, O. F. Sankey, A. L. Moore, T. A. Moore, D. Gust, G. Harris, and S. M. Lindsay, Science **294**, 571 (2001).

[11] A. D. Zhao, Q. X. Li, L. Chen, H. J. Xiang, W. H. Wang, S. Pan, B. Wang, X. D. Xiao, J. L. Yang, J. G. Hou, and Q. S. Zhu, Science **309**, 1542 (2005).

[12] P. Wahl, L. Diekhoner, G. Wittich, L. Vitali, M. A. Schneider, and K. Kern, Phys. Rev. Lett. **95**, 166601 (2005).

[13] J. R. Petta, D. G. Salinas, and D. C. Ralph, Appl. Phys. Lett. **77**, 4419 (2000).

[14] W. Y. Wang, T. Lee, I. Kretzschmar, and M. A. Reed, Nano Lett. **4**, 643 (2004).

[15] M. A. Reed, C. Zhou, C. J. Muller, T. P. Burgin, and J. M. Tour, Science **278**, 252 (1997).

[16] R. H. M. Smit, Y. Noat, C. Untiedt, N. D. Lang, M. C. van Hemert, and J. M. van Ruitenbeek, Nature **419**, 906 (2002).

[17] D. Dulic, S. J. van der Molen, T. Kudernac, H. T. Jonkman, J. J. D. de Jong, T. N. Bowden, J. van Esch, B. L. Feringa, and B. J. van Wees, Phys. Rev. Lett. **91** (2003).

[18] L. Gruter, F. Y. Cheng, T. T. Heikkila, M. T. Gonzalez, F. O. Diederich, C. Schonenberger, and M. Calame, Nanotechnology **16**, 2143 (2005).

[19] H. Park, J. Park, A. K. L. Lim, E. H. Anderson, A. P. Alivisatos, and P. L. McEuen, Nature **407**, 57 (2000).

[20] L. H. Yu and D. Natelson, Nano Lett. **4**, 79 (2004).

[21] L. H. Yu, Z. K. Keane, J. W. Ciszek, L. Cheng, M. P. Stewart, J. M. Tour, and D. Natelson, Phys. Rev. Lett. **93** (2004).

[22] J. Park, A. N. Pasupathy, J. I. Goldsmith, C. Chang, Y. Yaish, J. R. Petta, M. Rinkoski, J. P. Sethna, H. D. Abruna, P. L. McEuen, and D. C. Ralph, Nature **417**, 722 (2002).

[23] A. N. Pasupathy, R. C. Bialczak, J. Martinek, J. E. Grose, L. A. K. Donev, P. L. McEuen, and D. C. Ralph, Science **306**, 86 (2004).

[24] A. N. Pasupathy, J. Park, C. Chang, A. V. Soldatov, S. Lebedkin, R. C. Bialczak, J. E. Grose, L. A. K. Donev, J. P. Sethna, D. C. Ralph, and P. L. McEuen, Nano Lett. **5**, 203 (2005).

[25] W. J. Liang, M. P. Shores, M. Bockrath, J. R. Long, and H. Park, Nature **417**, 725 (2002).

[26] D. Chae, J. F. Berry, S. Jung, F. A. Cotton, C. A. Murillo, and Z. Yao, Nano Lett. **6**, 165 (2006).

[27] H. B. Heersche, Z. de Groot, J. A. Folk, H. S. J. van der Zant, C. Romeike, M. R. Wegewijs, L. Zobbi, D. Barreca, E. Tondello, and A. Cornia, Phys. Rev. Lett. **96**, 206801 (2006).

[28] L. P. Kouwenhoven, C. M. Marcus, P. L. McEuen, S. Tarucha, R. M. Westervelt, and N. S. Wintergreen, in *Mesoscopic Electron Transport*, edited by L. P. Kouwenhoven, G. Schon and L. L. Shon (Kluwer Academic Publishers, Dordrecht, 1996).

[29] K. K. Likharev, Proc. IEEE **87**, 606 (1999).

[30] S. De Franceschi, S. Sasaki, J. M. Elzerman, W. G. van der Wiel, S. Tarucha, and L. P. Kouwenhoven, Phys. Rev. Lett. **86**, 878 (2001).

[31] L. P. Kouwenhoven and L. I. Glazman, Physics World **14**, 33 (2001).

Chapter 2. Coulomb Blockade Effect and Higher-Order Tunneling Processes

2.1 INTRODUCTION

We are familiar with the fact that current increases linearly as an applied bias voltage increases across a macroscopic metallic object. Many intriguing questions naturally arise with the on-going miniaturization of electronic devices, such as: "Is Ohm's law still applicable to a *small* device? ". In this chapter, we will try to answer the above question and introduce basic ideas including the Coulomb blockade effect[1, 2] with examples in several different systems, cotunneling and the Kondo effect which are essential to understand the experimental observations in the rest of the chapters.

2.2 COULOMB BLOCKADE EFFECT

Let us consider a situation where electrons are added to an isolated and initially neutral conducting spherical island. After adding one electron to the island, the second electron needs to overcome the Coulomb charging energy of $E_c = e^2/2C$ to be added to the island, where e is the quantized charge of an electron and C is the capacitance of the spherical island ($C = 4\pi\varepsilon_0 R$ with radius R) (Fig. 2.1). As an example, the Coulomb charging energy for a metal sphere of 1 μm radius is 1.44 meV, which is negligible compared to the thermal energy at room temperature (~ 25 meV in energy). Therefore, this charging energy may not affect the transport phenomena at all at room temperature. However, when the same phenomenon is considered at low temperatures, for example, at 4.2 K (~0.3 meV in thermal energy), this Coulomb interaction should be taken into account.

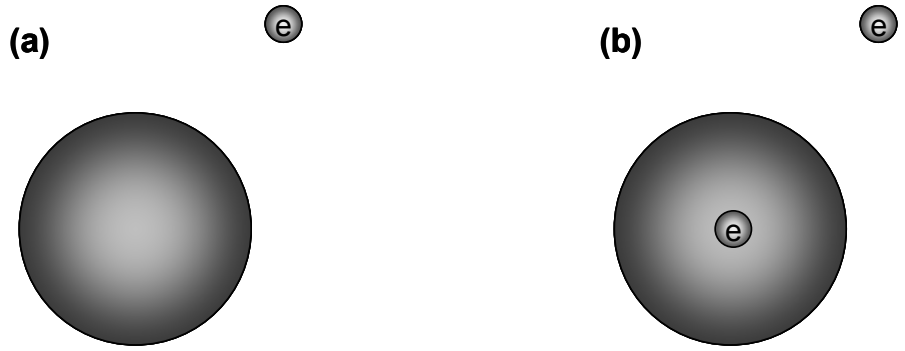

Figure 2.1 Addition of electrons to conducting sphere. (a) Neutral charge state. (b) One-electron charged state.

Now, let us consider a small island coupled to three terminals like a transistor, where two electrodes are weakly tunnel coupled to the island and the third electrode is capacitively coupled to the island as shown in Fig. 2.2 (a). When the tunneling resistance is much larger than the quantum of resistance h/e^2=25.813 kΩ, the number of charges is well-defined in the island. Here, capacitance values between the island and source, drain and gate are C_s, C_d and C_g,respectively. The electrostatic energy is given by

$$E = \frac{(Q - Q_{in})^2}{2C_\Sigma} ,$$

where Q is the number of charges in the island, $Q_{in} = V_g C_g$ is the continuous charge induced by the capacitively coupled gate, and C_Σ is the total capacitance ($C_\Sigma = C_s + C_d + C_g$). We can consider the electrostatic energy of the system for the following two different cases depending on the value of the induced charge. When the induced charge is an integer number ($Q_{in} = Ne$), the system is energetically most stable with the integer charge Q shown in Fig. 2.2 (b). On the other hand, when the induced

charge is half integer number ($Q_{in} = (N + \frac{1}{2})e$), the energy of the system is degenerate for the $Q = Ne$ and $Q = (N+1)e$ charge states (Fig. 2.2 (c)). In this case, the charge of the island fluctuates even at zero temperature. This simple argument describes qualitatively the Coulomb oscillation of the current as a function of the gate with a fixed small bias voltage. The peak in Fig. 2.2 (d) corresponds to the situation of Fig. 2.2 (c) and the valley in Fig. 2.2 (d) to the situation of Fig. 2.2 (b). Whenever an electron is added to the island by increasing the gate voltage, a peak is observed in measurement of current vs gate voltage. That is, the control of a fraction of a single-electron charge by the gate voltage enables a significant change of the conductance around a degeneracy point like a switch. This is why these three-terminal devices are named single-electron transistors (SETs).

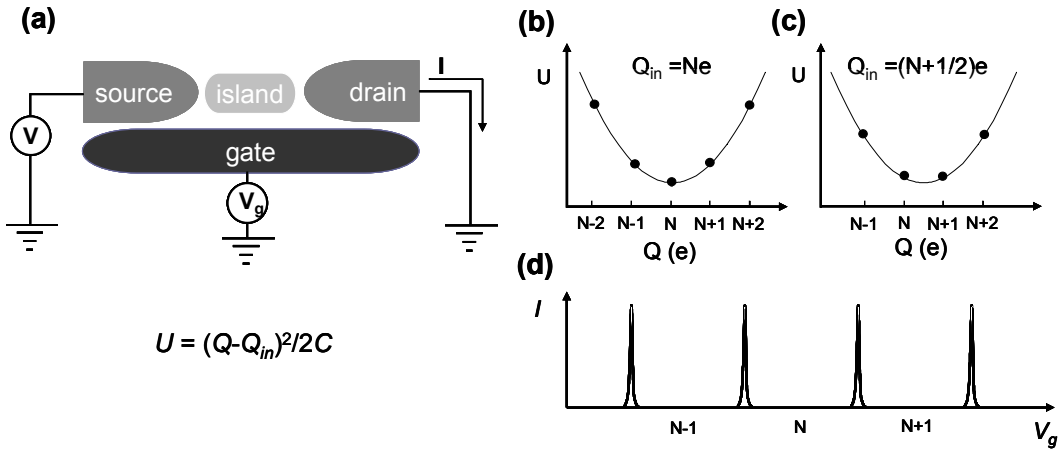

Figure 2.2 Single-electron transistor and Coulomb oscillation.
(a) Schematic diagram of a single-electron transistor. (b) Electrostatic energy as a function of discrete charge for integer induced charge. (c) Electrostatic energy as a function of discrete charge for half integer induced charge. (d) Current oscillation vs. gate voltage at a small bias voltage.

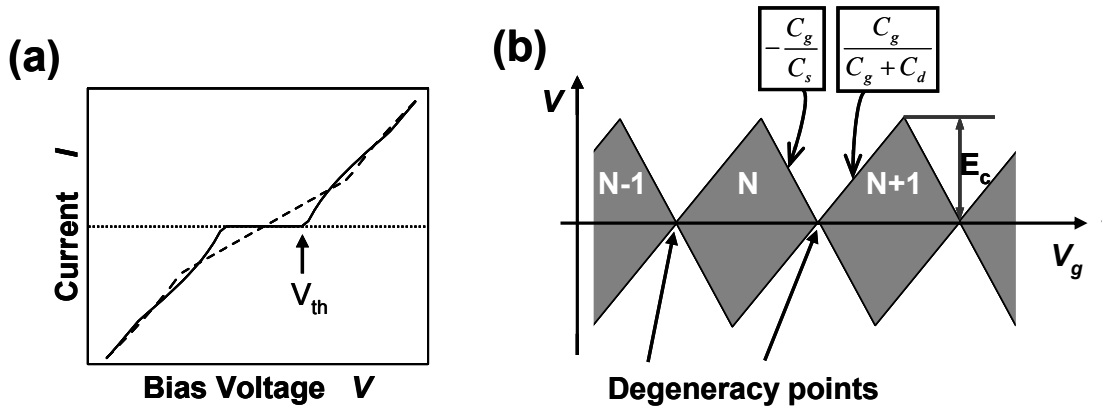

Figure 2.3 Coulomb blockade effect. (a) Characteristic current-bias (I-V) curves for integer charge (solid line) and half integer charge (dashed line). (b) Plot of differential conductance vs. gate and bias voltages. The grey diamond regions correspond to the suppression of conductance. Degeneracy points are marked by arrows. Two slopes are determined by ratios of the capacitances.

Figure 2.3 (a) shows typical current-bias voltage (*I-V*) curves of the system for the valley region (solid line) and the degenerate peak (dashed line) as illustrated in Fig. 2.2 (d). The current is suppressed at small bias voltage in the valley region in Fig. 2.2 (d) since the tunneling event of an electron is prevented due to the repulsive Coulomb interaction. By differentiating *I-V* curves for different gate voltages, we can get a plot of differential conductance as a function of gate and bias voltages in Fig. 2.3 (b). The grey area corresponds to the blockade region and the arrows point to the degeneracy points in the current-gate plot in Fig. 2.2 (d).

The Coulomb blockade region in a two-dimensional conductance plot is defined by two characteristic slopes, which are determined by ratios of capacitance values[3]. If the

drain is grounded, the negative slope becomes $-\frac{C_g}{C_s}$ and the positive slope becomes $\frac{C_g}{C_g + C_d}$ as shown in Fig. 2.3 (b).

The above description does not include any quantum behavior except the tunneling of electrons through the island. It is expected that if the island size is small enough compared to the wavelength of the electron in the island, the energy levels are quantized due to quantum confinement when electrons reside in an island. This effect has to be taken into account.

Figure 2.4 (a) illustrates the schematic energy diagram of a quantum dot taking into account these quantum states. The solid lines represent the ground states of each charged state. The dotted lines illustrate quantized excited states. The gate is utilized to align the ladder of quantum states with respect to source and drain chemical potentials. The bias voltage between the source and drain electrodes opens an energy window, $eV = \mu_s - \mu_d$. Any state within this window can contribute to current flow. Initially, an electron tunnels through a ground state when the bias voltage is small. When the bias voltage is increased, excited states enter this energy window. These excited states contribute extra tunneling channels. The current increases stepwise whenever an excited state enters the bias window as illustrated in Fig. 2.4 (b). These features correspond to conductance peaks as manifested by dotted lines along the boundaries of the Coulomb diamonds in the two dimensional plot of differential conductance as illustrated in Fig. 2.4 (c).

These excitation features change in general with respect to the charge state of the quantum dot. The excited states of the N electron-charged island illustrated by two dotted lines ending in the N electron state change into the excited states of the N+1 electron

system indicated by dotted lines terminated in the N+1 electron-charged state (Fig. 2.4 (c)).

The addition energy, which is needed to add one more electron to a quantum dot, consists of the charging energy and the energy level spacing between two adjacent electronic states. The value is measured as illustrated in Fig. 2.4 (c). The energy of the excitation is measured from the horizontal bias axis to the intersection of the Coulomb

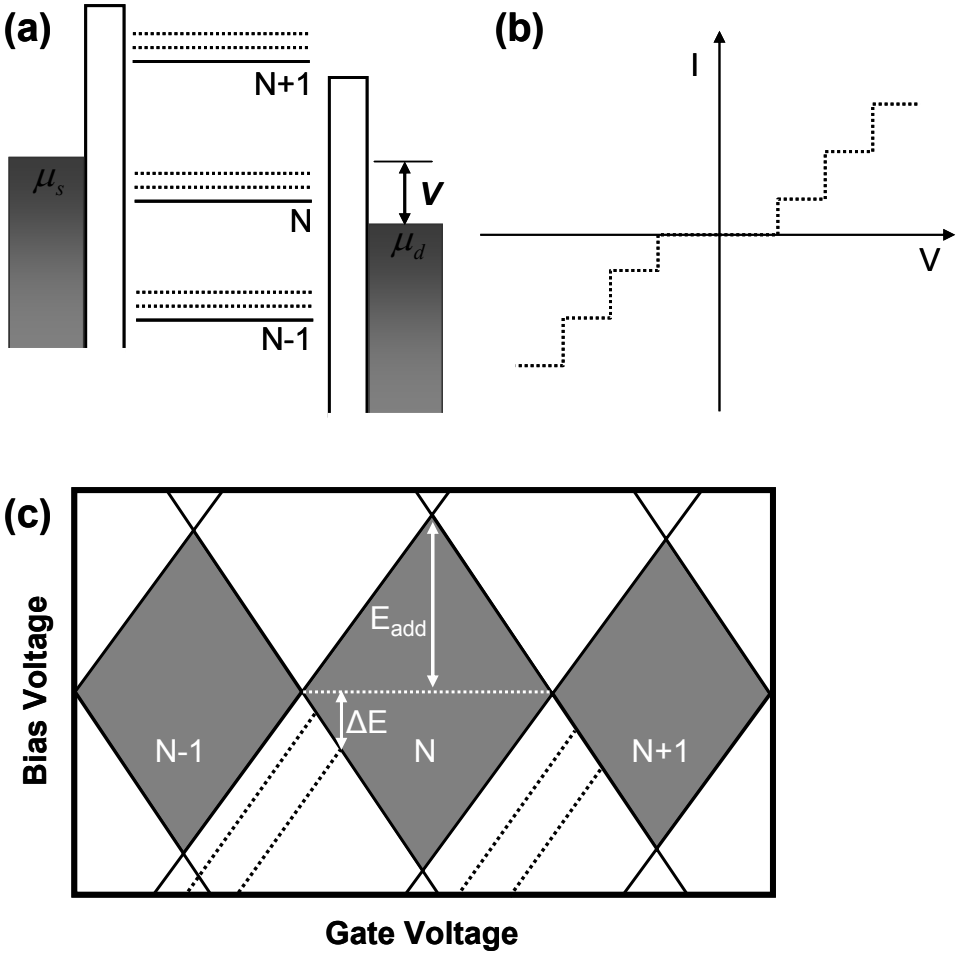

Figure 2.4 Tunneling through discrete energy levels.
(a) A schematic energy diagram of a quantum dot. Solid (dotted) lines represent the ground (excited) states. (b) Stepwise *I-V* characteristics.
(c) Differential conductance vs. bias and gate voltages.

diamond boundary line and the excitation line in the conductance plot as illustrated in Fig. 2.4 (c). Based on the above description, we can utilize the electron transport measurement as a spectroscopic tool to understand electronic structures of a small object in the Coulomb blockade regime.

2.3 EXAMPLES OF SINGLE-ELECTRON TRANSISTORS

The non-linear *I-V* characteristics were observed by Giaver and Zeller in 1968[4] and Lambe and Jaklevic in 1969[5] in thin films containing a number of small metallic islands indicating the Coulomb blockade effect through the ensemble of the metallic islands. A rapid advance in device fabrication using electron-beam lithography and thin-film processing allows the realization of well-defined SETs in various different ways. Fulton and Dolan in 1987[6] demonstrated a single-electron transistor with an aluminum island connected to leads through thin aluminum oxide tunnel barriers as shown in Fig. 2.5 (a). Since then, metallic island systems have been studied intensively including superconducting systems[7, 8]. More recently, Ralph group at Cornell introduced a simple fabrication method[9] for an SET incorporating a metallic island located in a small gap, which is fabricated by the electromigration technique[10].

Another attempt has been carried out with semiconducting heterostructures[11-13]. The electrons form a two-dimensional electron gas (2DEG) at the interface of a GaAs/AlGaAs heterostucture (Fig. 2.5 (b)). The electrons can be fully confined in the z-direction (perpendicular to the interface) for a proper controlling of the electron density and they can move freely in the x-y plane with a mean free path of order 100 μm. Metallic gates are then patterned on the surface of the sample by electron-beam lithography. By applying negative voltages on the metallic gates, a droplet of electrons is formed in a nearly isolated area about 100 nm underneath the surface of sample. This

droplet is connected to the source and drain 2DEG systems with tunnel barriers tuned by the voltage applied to the metallic gates. If the dimension of 2DEG droplet is comparable to the Fermi wavelength, the quantum confinement is important and can be observed usually at low temperature (~100 mK) in a dilution refrigerator. Therefore, the droplet of electrons is called a quantum dot.

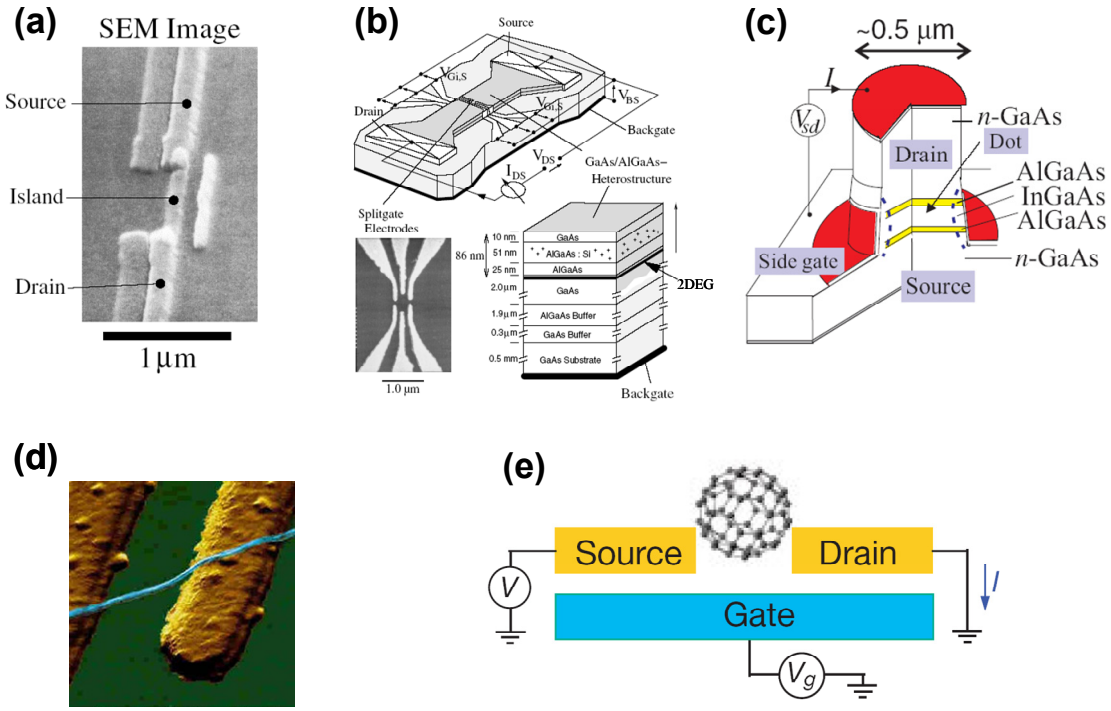

Figure 2.5 Examples of single-electron transistors.
(a) Metallic island (from Ref. 3). (b) Quantum dot (from Ref. 3). (c) Quantum dot pillar (from Ref. 14). (d) Single-wall carbon nanotube (from Ref. 17). (e) Single molecule (from Ref. 22).

The quantum dot pillar[14-16] is another system defined vertically by etching the semiconducting heterostructure (Fig. 2.5(c)). The confined potential of a disk-shaped 2DEG system can be approximated by a harmonic potential and the number of electrons

can be controlled down to a few electrons in the system. The symmetry of the two dimensional cylindrical and harmonic potential leads to a two-dimensional shell filling according to Hund's rule, similar to the atomic physics.

Single-wall carbon nanotubes[17] have also been made into SETs. These devices have shown many interesting phenomena including shelling filling[18], electron-hole symmetry[19], and the orbital Kondo effect[20] (Fig. 2.5 (d)). The system is also actively utilized to realize coupled quantum dots analogous to that in 2DEG[21]. Our interests in SWNTs will be described in detail in Chapter 7.

Finally, single-molecule transistor is one of hot research areas even though challenges and controversies coexist. Since the SET incorporating C_{60} was demonstrated by H. Park and his collaborators in 2000[22], extensive investigations on molecular transistors have been carried out (Fig. 2.5 (e)). Single-molecule transistor systems enable us to study individual molecules by tuning the charge state of the molecules with a gate voltage in the Coulomb blockade regime.

2.4 HIGHER-ORDER TUNNELING PROCESSES AND THE KONDO EFFECT

Single-electron tunneling is a good approximation for a weakly-tunnel coupled quantum dot. However, when the quantum dot is strongly coupled to the leads, higher-order tunneling processes[23] exist even in the Coulomb blockade region. The higher-order process is sometimes called "cotunneling" because two or more electrons are involved in the process simultaneously. For instance, when one electron enters a dot through a tunnel barrier via a quantum state (Fig. 2.6 (b)) and another electron leaves the same state coherently, the cotunneling is called "elastic" cotunneling. When cotunneling arises via two different states as shown in Fig. 2.6 (c), it is called "inelastic" cotunneling. In Fig. 2.6 (a), the dark grey region corresponds to elastic cotunneling through the ground state

of a quantum dot while the light grey zone corresponds to inelastic processes via the ground state and an excited state (dotted line). Observation of inelastic cotunneling process was first reported that it occurs in 2DEG quantum dots[24].

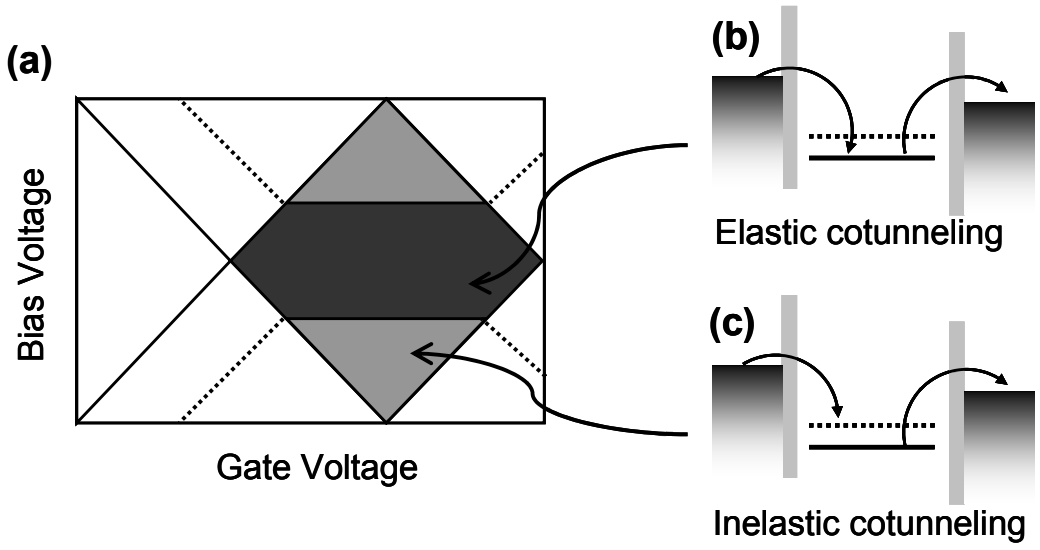

Figure 2.6 Cotunneling processes. (a) Plot of differential conductance in the presence of cotunneling processes. (b) "Elastic" cotunneling. (c) "Inelastic" cotunneling.

We now consider a cotunneling process by taking account of the spin contribution. Suppose that the island and the leads are strongly coupled and there exists an unpaired spin in the island (Fig. 2.7 (a)). The localized spin is antiferromagnetically coupled to spin of conduction electron in the left electrode by the spin exchange interaction. The localized spin can escape from the well state in the island virtually to the right electrode since the Heisenberg uncertainty principle allows the process quantum mechanically for a short time around $h/|\varepsilon_o|$, where h is the Plank constant and ε_o is the "depth" of the well state (Fig. 2.7 (b)). Within this time scale, another electron from the

left electrode may occupy the same well state with an opposite spin (Fig. 2.7 (c)). This mechanism makes the local spin effectively flip. The whole process could be understood as a cotunneling process where two electrons are coherently involved with the spin flip due to an exchange interaction. Many such events introduce a tunneling density of states aligned to the Fermi energy of the two electrodes, leading to an enhancement of conductance or resonance at zero bias at low temperatures. This is known as the Kondo effect in single-electron devices[25]. We note that the same Kondo screening of a local spin by nearby electrons suppresses the conductance in a classical metallic system containing magnetic impurities. The Kondo effect is significant below a characteristic temperature, the so-called Kondo temperature, which is a measure of the exchange interaction. The Kondo temperature, T_K is approximately estimated by the full width at half maximum of the Kondo resonance[26],

$$\text{FWHM} \sim 2k_B T_K / e .$$

SETs allows us to investigate the Kondo effect in a more controllable way, compared to the conventional Kondo system, in which dilute magnetic impurities are embedded in a metal host. Since the number of electrons in SET is changed one by one by a capacitively coupled gate, Kondo/non-Kondo resonance can generally be manipulated by controlling the odd/even number of electrons. An exceptional case is discussed in Chapter 6. In addition, the exchange coupling between the local spin in the island and free electrons in electrodes can be tuned by the gate voltage[27]. The Kondo temperature[28] representing the exchange strength is

$$T_K \sim (U\Gamma)^{1/2} e^{-\pi(\mu-\varepsilon_0)/2\Gamma},$$

where U is the on-site electron repulsion energy, Γ is the width of the energy level, and μ is the Fermi energy of the electrodes. For instance, if we decrease the "distance" between the energy level and the Fermi energy using the gate voltage from a Coulomb valley

toward a degeneracy point, the Kondo temperature increases, resulting in increasing the width of the Kondo resonance. The relevant phenomena are presented in Chapter 5 and Chapter 6.

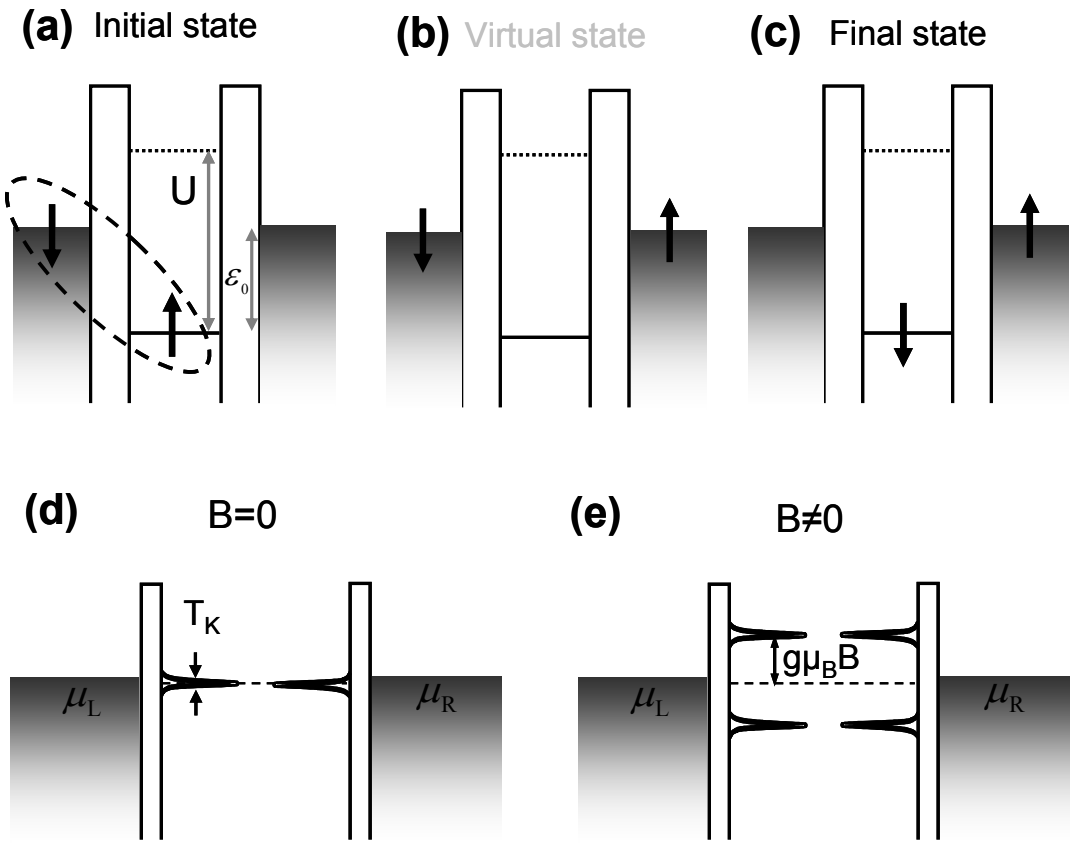

Figure 2.7 The Kondo effect in a single-electron transistor. (a) The localized spin is antiferromagnetically coupled to spins of conduction electrons in the leads due to exchange interaction. (b) The Heisenberg uncertainty principle allows the localized spin to escape the well state virtually. (c) The well state is occupied by an opposite spin. (d) The Kondo effect leads to the tunneling density of states aligned to the Fermi energy of leads, resulting in the Kondo resonance. (e) The resonance peak is spilt under an external magnetic field with a magnitude of $2g\mu_B B/e$.

There are two criteria to determine whether the zero-bias resonance can be attributed to the Kondo effect or not. One fingerprint of the Kondo resonance is the Zeeman splitting of a resonance peak in a conductance plot under an applied magnetic field. The magnitude of the splitting is $2g\mu_B B/e$, where g is the Lande g factor (~2 for a free electron), μ_B is the Bohr magneton and B is the external magnetic field[29]. When an external magnetic field is applied at a zero bias, there is no tunneling state available aligned to Fermi energies of leads as illustrated in Fig. 2.7 (e). Thus, the conductance is suppressed. As the bias voltage is increased and the split density of states enters the bias window, it increases the conductance. When the right and left split density of states are aligned, it gives rise to a conductance peak at either positive or negative bias voltage. Therefore, the splitting of the resonance peak results in twice the ordinary Zeeman splitting. The example is shown in section 5.3 in Chapter 5. The other signature of the Kondo resonance is the logarithmic temperature dependence. The conductance peak height follows a functional form[30]:

$$G_K = G_0(1+(2^{-s}-1)(T/T_K)^2)^{-s},$$

where G_0 is a constant, s is an asymptotic value of 0.22 for spin ½, and T_K is the Kondo temperature.

REFERENCES

[1] L. P. Kouwenhoven, C. M. Marcus, P. L. McEuen, S. Tarucha, R. M. Westervelt, and N. S. Wintergreen, in *Mesoscopic Electron Transport*, edited by L. P. Kouwenhoven, G. Schon and L. L. Sohn (Kluwer Academic Publishers, Dordrecht, The Netherlands, 1996).

[2] K. K. Likharev, Proc. IEEE **87**, 606 (1999).

[3] J. Weis, in *CFN Lectures on Functional Nanostructures* edited by K. Busch, A. Powell, C. Röthig, G. Schön and J. Weissmüller (Springer Berlin/Heidelberg, 2005), Vol. 1.

[4] I. Giaever and H. R. Zeller, Phys. Rev. Lett. **20**, 1504 (1968).

[5] J. Lambe and R. C. Jaklevic, Phys. Rev. Lett. **22**, 1371 (1969).

[6] T. A. Fulton and G. J. Dolan, Phys. Rev. Lett. **59**, 109 (1987).

[7] T. M. Eiles, J. M. Martinis, and M. H. Devoret, Phys. Rev. Lett. **70**, 1862 (1993).

[8] M. Tinkham, *Introduction to Superconductivity* (McGraw-Hill, New York, 1996).

[9] K. I. Bolotin, F. Kuemmeth, A. N. Pasupathy, and D. C. Ralph, Appl. Phys. Lett. **84**, 3154 (2004).

[10] H. Park, A. K. L. Lim, A. P. Alivisatos, J. Park, and P. L. McEuen, Appl. Phys. Lett. **75**, 301 (1999).

[11] J. H. F. Scottthomas, S. B. Field, M. A. Kastner, H. I. Smith, and D. A. Antoniadis, Phys. Rev. Lett. **62**, 583 (1989).

[12] L. I. Glazman and R. I. Shekhter, J. Phys. Condens. Matter **1**, 5811 (1989).

[13] P. L. McEuen, E. B. Foxman, U. Meirav, M. A. Kastner, Y. Meir, N. S. Wingreen, and S. J. Wind, Phys. Rev. Lett. **66**, 1926 (1991).

[14] S. Tarucha, D. G. Austing, T. Honda, R. J. vanderHage, and L. P. Kouwenhoven, Phys. Rev. Lett. **77**, 3613 (1996).

[15] L. P. Kouwenhoven, T. H. Oosterkamp, M. W. S. Danoesastro, M. Eto, D. G. Austing, T. Honda, and S. Tarucha, Science **278**, 1788 (1997).

[16] T. H. Oosterkamp, J. W. Janssen, L. P. Kouwenhoven, D. G. Austing, T. Honda, and S. Tarucha, Phys. Rev. Lett. **82**, 2931 (1999).

[17] C. Dekker, Physics Today **52**, 22 (1999).

[18] W. J. Liang, M. Bockrath, and H. Park, Phys. Rev. Lett. **88**, 126801 (2002).

[19] P. Jarillo-Herrero, S. Sapmaz, C. Dekker, L. P. Kouwenhoven, and H. S. J. van der Zant, Nature **429**, 389 (2004).

[20] P. Jarillo-Herrero, J. Kong, H. S. J. van der Zant, C. Dekker, L. P. Kouwenhoven, and S. De Franceschi, Nature **434**, 484 (2005).

[21] M. J. Biercuk, S. Garaj, N. Mason, J. M. Chow, and C. M. Marcus, Nano Lett. **5**, 1267 (2005).

[22] H. Park, J. Park, A. K. L. Lim, E. H. Anderson, A. P. Alivisatos, and P. L. McEuen, Nature **407**, 57 (2000).

[23] D. V. Averin and Y. V. Nazarov, in *Single Charge Tunneling: Coulomb Blockade Phenomena in Nanostructures*, edited by H. Grabert and M. H. Devoret (Plenum Press and NATO Science Affairs Division, New York, 1992).

[24] S. De Franceschi, S. Sasaki, J. M. Elzerman, W. G. van der Wiel, S. Tarucha, and L. P. Kouwenhoven, Phys. Rev. Lett. **86**, 878 (2001).

[25] L. P. Kouwenhoven and L. I. Glazman, Physics World **14**, 33 (2001).

[26] W. G. van der Wiel, S. De Franceschi, T. Fujisawa, J. M. Elzerman, S. Tarucha, and L. P. Kouwenhoven, Science **289**, 2105 (2000).

[27] S. M. Cronenwett, T. H. Oosterkamp, and L. P. Kouwenhoven, Science **281**, 540 (1998).

[28] N. E. Bickers, Rev. Mod. Phys. **59**, 845 (1987).

[29] Y. Meir, N. S. Wingreen, and P. A. Lee, Phys. Rev. Lett. **26**, 2601 (1993).

[30] D. Goldhaber-Gordon, J. Gores, M. A. Kastner, H. Shtrikman, D. Mahalu, and U. Meirav, Phys. Rev. Lett. **81**, 5225 (1998).

Chapter 3. Device Fabrication and Experimental Setup

3.1 INTRODUCTION

Advances in technology have enabled the fabrication of nanoscale devices. These nanoscale devices allow us to access a fundamentally new regime, which is not accessible with classical macroscopic structures. It drives researchers to investigate many intriguing scientific issues as well as possible new applications. Electron-beam lithography is one of the most advanced tools for fabricating features down to 5 nm in size while optical lithography is utilized to pattern micron- or larger-sized features. In our study, electron-beam lithography and optical lithography are combined to make devices more efficiently.

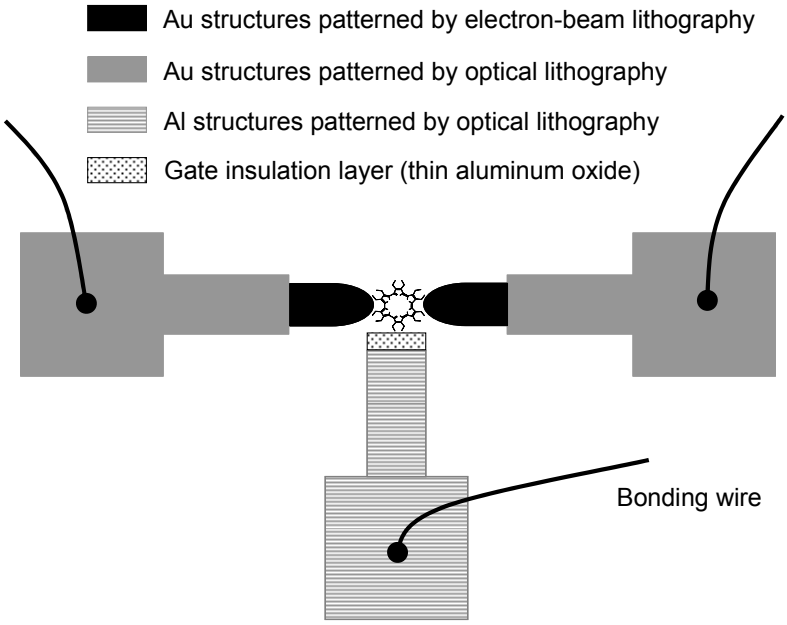

Figure 3.1 Schematic diagram of a single-molecule transistor.

Figure 3.1 shows a schematic diagram of a single-molecule transistor (not scaled). It consists of the source and drain electrodes connected to a molecule and a gate, which is capacitively coupled to the molecule through an insulation layer. There are two key techniques to realize the device. First, we have adopted the electromigration technique[1] to fabricate a small gap in a Au nanowire. Second, we have untilized thin aluminum oxide layer to achieve an effective capacitance coupling between the inserted molecule and the gate electrode. In general, coarse structures are patterned by optical lithography and fine Au nanowires are made using electron-beam lithography.

In this chapter, the fabrication procedure is described first. Then, experimental setup is presented. Finally, the in-situ fabrication of molecular transistors using the electromigration technique is described.

3.2 DEVICE FABRICATION

Figure 3.2 shows the schematic diagram of the procedure to fabrication of a metal structure using either optical lithography or electron-beam lithography. We use a bilayer for both lithographies because of the following two reasons: First, a bilayer resist helps to lift off the residual edge structures, which usually remain after lift-off if only a single layer resist is used. Since some amount of metal is deposited on the wall of the single resist during metal deposition, it creates residual metal at the boundaries of designed structures. Second, the undercut structure in the bilayer resist enables the shadow evaporation as will be explained later. We expose the bilayer coated substrate through a mask to UV light in optical lithography or to an electron beam in electron-beam lithography according to a pre-designed pattern. The exposed pattern is developed in a proper developer to remove the exposed resist. Metal deposition follows with either

thermal evaporation or electron-beam evaporation. The final step is the lift-off in a proper solvent to remove the rest of metal structures except the designed structures.

The procedure is described sequentially in the following subsections from the fabrication point of view as follows: First, Au coarse structures are fabricated by optical lithography and metal deposition (Subsection 3.2.1). Second, Al gate are then made in the similar way as Au coarse structures following an oxidation procedure for the gate application (Subsection 3.2.2). Third, Au nanowire is patterned using electron-beam lithography and metal deposition on top of the Al gate (Subsection 3.2.3).

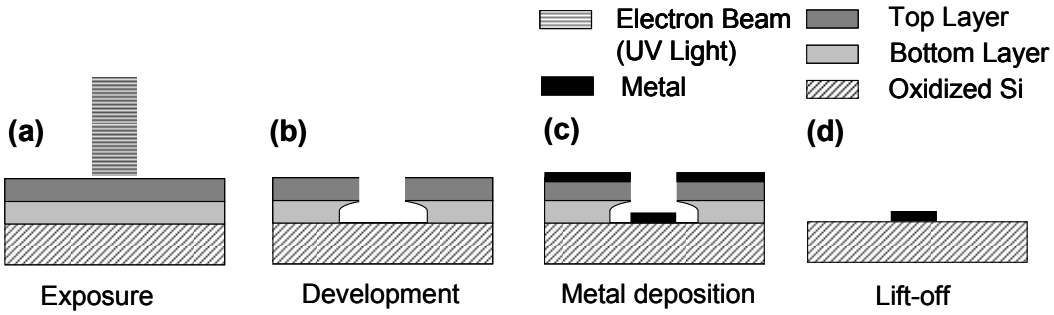

Figure 3.2 Schematic description of lithography. (a) Exposure. (b) Development. (c) Metal deposition. (d) Lift-off.

3.2.1 Fabrication of gold coarse structures using optical lithography

In this subsection, a description of conventional fabrication procedures using optical lithography for coarse Au structures is introduced.

Piranha Clean

Piranha clean is applied to remove organic contaminants on the surface of 4 inch silicon wafers before optical lithography. The cleaning procedure is as follows: wafers

are placed in a 1:2 H_2O_2 H_2SO_4 solution for 5 minutes, and then rinsed with distilled (DI) water for 5 minutes. The wafers are then dried with dry nitrogen gas.

Bi-layer photoresist and photolithography

Bi-layer resist with the LOR-3A resist from MicroChem (www.microchem.com) as a bottom layer in combination with AZ5214 photoresist as a top layer is used to achieve a reliable lift-off process. The recipe is as follows: LOR-3A is spin-coated on a 4 inch wafer at 3000 RPM for 35 seconds. The wafer is then baked in a hotplate at 170 ^oC for 5 minutes. Next, AZ5214 photoresist is spin-coated at 3000 RPM for 40 seconds. The coated wafer is baked at 115 ^oC for 2 minutes. After the bilayer coated wafer is exposed using Karl Suss mask aligner for 25 seconds, the wafer is baked at 120 ^oC for 5 minutes and then developed in the CD-26 developer (MicroChem) for 60 seconds. Finally, it is rinsed in DI water and blow-dried.

Cr and Au thermal evaporation

Cr and Au are evaporated in a thermal evaporator under the vacuum of 2 x 10^{-6} torr. 5 nm Cr is evaporated first as a sticking layer, then Au is evaporated to a thickness of about 30 nm.

Lift-off procedure

The next step is lift-off. LOR-3A and photoresist are lifted off using MicroChem's remover PG, which is a NMP (N-methylpyrrolidone) based solvent. First, the wafer is immersed in the remover PG that is heated to 80 ^oC. The metal-coated wafer is lifted off by blowing the wafer with a pipette while stirring the PG after 10 minutes of soaking. The wafer is then rinsed in fresh pre-heated remover for 10 minutes to remove residual photoresist. It should be emphasized that the remover is heated for clean lift-off before the wafer is immersed. After that, the wafer is rinsed in boiling acetone and isopropanol consecutively for 10 minutes each. The wafer is finally blown with dry

nitrogen gas. Scanning electron micrographs of the resultant metal structures are shown in Fig. 3.3.

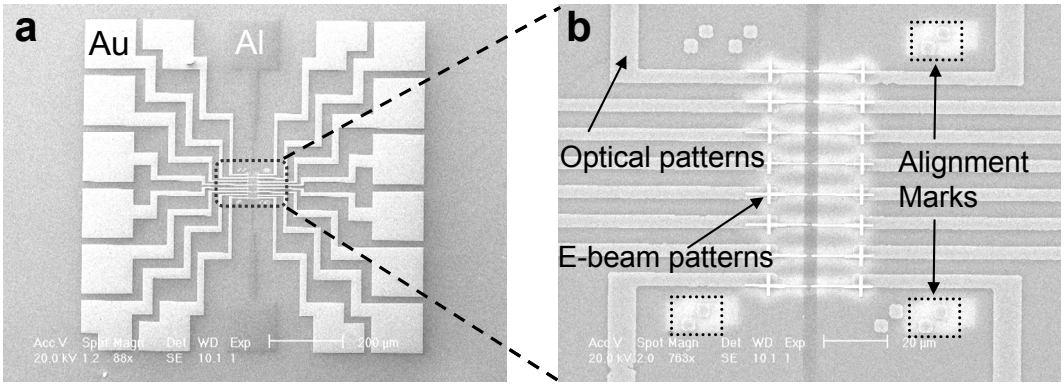

Figure 3.3 Scanning electron micrographs of a device. (a) Coarse structures of Au and Al fabricated by optical lithography. (b) Magnified image of the central area fabricated by electron-beam lithography.

3.2.2 Fabrication of aluminum gates using optical lithography

An aluminum oxide gate is utilized to achieve a strong gate modulation. For ordinary silicon back gate with a typical 200 to 500 nm thick silicon dioxide, the gating effect is weak because the electric field is mostly screened by nearby electrodes since the gap is the order of a nanometer or less for single-molecule devices. Therefore, the trapped molecule in the gap has almost no chance to "see" the applied gate voltage. Although we reduce the thickness of the silicon dioxide to a few nm, we cannot achieve a low gate leakage. Because of the thickness of insulation layer, rather high gate voltage is required to achieve a reasonable gating effect. However, gate leakage current occurs from Si substrate to the Au coarse bonding pads connected to contact leads. It leads to the situation that the resultant current through molecules cannot be measured reliably

because of this leakage current. On the other hand, a strong gating effect can be achieved with Al gate, which has a very thin aluminum oxide layer, at a reasonably low gate voltage. We introduce our recipe to make reliable Al gate based on previous results[2-4] by other groups. The requirements of an Al gate are as follows: First, the leakage current through the thin aluminum oxide must be reasonably small before and after electromigration. Second, the breakdown voltage should be reasonably high (for instance, 4 V in our case) to achieve good gate modulation. A systematic study is reported in Ref .4.

Photoresist system and photolithography for Al gate

In addition to following the same procedure for coarse Au structures as described in subsection 3.2.1, a standard alignment procedure is carried out with a mask aligner with respect to the existing coarse Au structures.

Al evaporation

Al evaporation is carried out in an electron-beam evaporator with a good vacuum (< 1 x 10^{-7} torr) and with a sample stage cooled by liquid nitrogen in order to achieve a high quality (good surface morphology and few impurities) Al film. The liquid nitrogen jacket for the vacuum chamber should be filled before the cooling sample stage is filled with liquid nitrogen in order to trap the moisture and contaminants in the jacket and not on the surface of the wafer. The liquid nitrogen is then slowly introduced from one of the two outlets and drained through the other. The flow of liquid nitrogen is adjusted until the liquid is seen from the outlet. After that, it is allowed to flow for about 20 minutes to ensure that the cooling stage in the chamber reaches the liquid nitrogen temperature. Al is pre-evaporated with the shutter closed to clean the Al source, and then it is evaporated on the wafer to about 20 to 30 nm in thickness. It takes overnight for the wafer to warm up to room temperature by flowing nitrogen gas through the same outlets.

Lift-off

The exact same procedure for the coarse Au structures is followed. Refer to Subsection 3.2.1.

Oxidation of Al gate

A reliable aluminum oxide layer is essential to make an Al gate work. We intentionally carry out oxygen plasma oxidation at a pressure of 7 psi with a mixture of 25% oxygen and 75% argon in a plasma cleaner (Fischione Instruments Model 1020) for 30 minutes. After the nanoconstrictions are fabricated as will be described below, the leakage current is measured between either the source or drain electrodes and the Al gate across the thin oxide layer. In our device geometry, the leakage current is less than 10^{-11} A at 3 V at room temperature as shown in Fig. 3.4. This leakage current is acceptable compared to the signal current, which is usually in the range of 10^{-11} A to 10^{-9} A around a bias voltage of 0.1 V. This leakage current is significantly improved at low temperature.

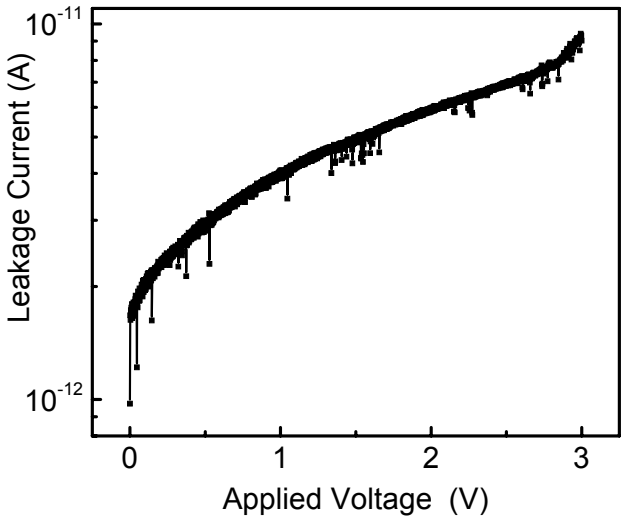

Figure 3.4 Leakage current of the Al gate at room temperature.

3.2.3 Fabrication of nanowires with nanoconstrictions

In this subsection, a procedure of fabrication for nanoconstrictions is described. Electron-beam lithography is applied to pattern Au nanowires with 100 nm constrictions on top of an Al gate electrode. After bi-layer polymethyl methacrylate (PMMA) is exposed by electron-beam lithography and developed, shadow evaporation is adopted to make fine structures reliably connected to the Au coarse structures. Careful lift-off should be carried out because there is no sticking layer like Cr for the fine structures.

PMMA bi-layer and electron-beam lithography

Two homemade PMMA resists are used for the PMMA bi-layer. A 35 K PMMA (Acros Organics) 8% in weight in chlorobenzene and a 996 K PMMA(Aldrich) 4% in weight in chlorobenzene are prepared by stirring the solutions for at least 24 hours. The 35 K PMMA is used to achieve a better undercut for shadow evaporation. The following is the procedure: First, 35K PMMA is spin-coated at 6000 RPM as a bottom layer on a diced substrate (2x2 cm^2), resulting in 430 nm in film thickness. It is baked in a convection oven at 170 ^oC for 30 minutes. Next, a 996 K PMMA is spin-coated at the speed of 6000 RPM as the top layer, resulting in 370 nm in film thickness. It is then baked at 170 ^oC for 30 minutes.

Fine nanowire structures having narrow constrictions of 100 nm or less are fabricated by electron-beam lithography using 20 keV electron beam in Raith50 pattern generator equipped with laser sample stage. The features are aligned with respect to existing structures fabricated by optical lithography. We usually use 220 $\mu C/cm^2$ as a dose factor. The electron beam-exposed patterns on the substrate are then developed for 60 seconds in a 3:1 mixture of 2-isopropanol:methyl-isobutyl-ketone (IPA:MIBK) and rinsed for 60 seconds in IPA. Finally, the developed pattern is blown dry with dry nitrogen gas.

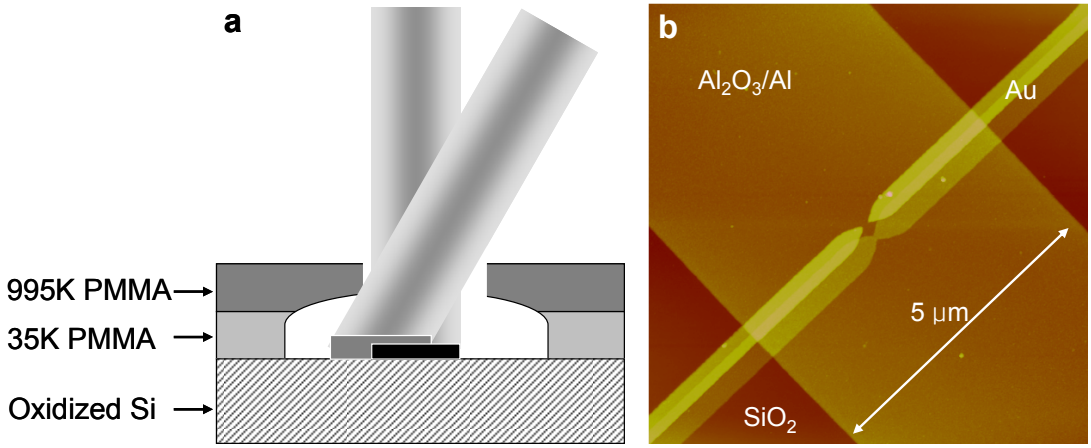

Figure 3.5 Shadow evaporation. (a) Evaporation is carried out in two steps; after the 15 nm thin Au layer is deposited perpendicular to the sample surface, the 70 nm thick Au layer is deposited at an angle. (b) Atomic force micrograph of a resultant structure.

Shadow evaporation

Au nanoconstrictions of 100 nm or less in width and 15 nm in thickness are fabricated on top of the 5 μm wide Al gate strip. The thickness of the Au constriction is critical for reliable electromigration, which should occur at low bias voltage (below 1.2 V) in order to create a small gap corresponding to the size of molecule. However, 15 nm thick Au strips cannot maintain electric continuity across the step at the edge of the 30 nm thick Al gate. In order to solve this problem, another thick Au layer (about 70 nm) is thermally evaporated at an angle without breaking the vacuum (Fig. 3.5 (a)). As shown in Fig. 3.5 (b), the thick layer is continuous over the Al edge step but the layer is not connected around the nano constriction.

Lift-off

Lift-off procedure is carried out very carefully because the structure does not have any sticking layer such as Cr. Diced devices are soaked in a beaker filled with boiling

acetone indirectly heated in a water-filled flask for 10 minutes. Then, the devices are gently shaken until the deposited Au film is peeled off. A pipette or sonicator cannot be used. Next, the devices are immersed again in boiling acetone for rinsing for 10 minutes at least three times to make a clean lift-off. Finally, the fabricated structures are rinsed in IPA and blow-dried with dry nitrogen gas.

3.3 EXPERIMENTAL SETUP

Transport is measured most times at 4.2 K with a dip-stick type cryostat built by Desert Cryogenics. The base temperature can be lowered down to 1.5 K by evacuating the 1 K pot. We also use a dilution refrigerator (Minikelvin 126-TOF) built by Leiden Cryogenics equipped with a 9 T superconducting magnet. The whole measurement system is electrically isolated from the building's power ground, which contains high frequency interferences, using a power isolation transformer.

Figure 3.6 shows transport measurement schematics of both dc and ac lock-in measurements. The measurement setup consists of a current preamplifier (DL Instruments 1211), a lock-in amplifier (Standford Research Systsems SR830), a data acquisition card (National Instruments DAC PCI-6052E), and a temperature controller (Lake Shore Cryotronics 331).

For dc current-voltage measurement, a bias is applied through a low-pass RC filter with a cut-off frequency ($f = 1/2\pi RC$, where R=20 Ω and C=470 μF) at 17 Hz and a divider. The voltage divider is used to improve the DAC resolution. For example, the 16 bit DAC has about 0.3 mV in resolution. The resolution is improved by the voltage divider even at the expense of reduced voltage range. If we use a 100x voltage divider, the resolution becomes 3 μV and the bias range is reduced from ±10 V to ±0.1 V. The current is amplified by the DL 1211 preamplifier. The output voltage from the

preamplifier is read by an NI-DAC in a personal computer. The temperature is monitored and controlled by LakeShore temperature controller 331 during the experiment via GPIB communication through a thermometer and heater attached on a sample holder in the cryostat.

The overall setup of ac lock-in measurement is similar to the dc measurement. An additional sinusoidal excitation bias voltage from a lock-in amplifier is added to the existing bias divider for the dc bias through a 1000x divider to measure the differential conductance (dI/dV). The resultant current is amplified with the DL 1211 preamplifier and the output signal voltage is feed to the lock-in amplifier to measure the ac current, which is attributed to the sinusoidal excitation bias voltage. Finally, the amplified voltage from the lock-in is read by the NI-DAC to measure the resultant differential conductance.

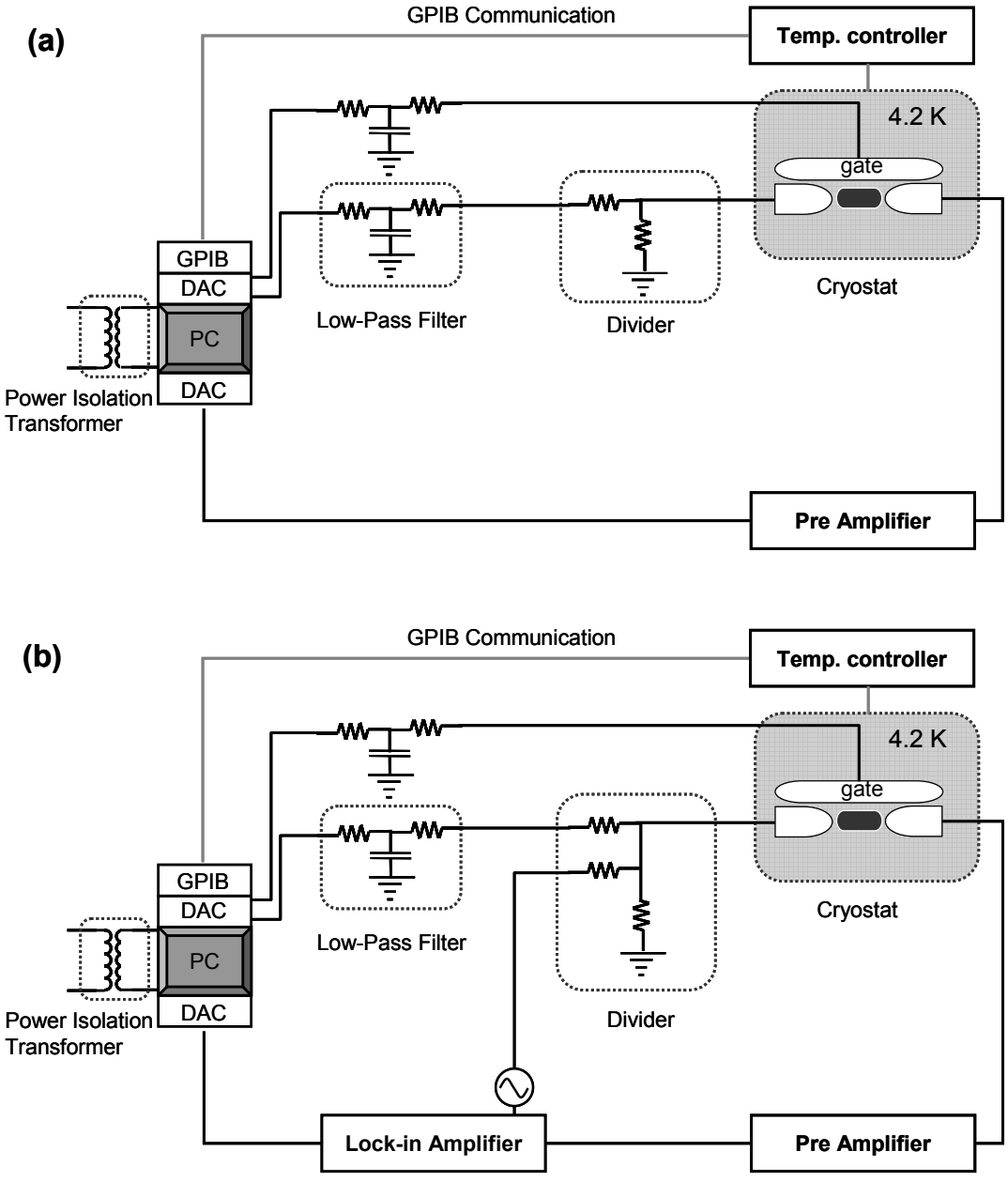

Figure 3.6 Schematic diagrams of measurement setups. (a) dc measurement setup. (b) ac lock-in measurement setup.

3.4 ELECTROMIGRATION AND PREPARATION OF MOLECULAR DEVICES

The electromigration technique is applied to fabricate molecular devices in-situ. The nanowires are first cleaned in oxygen plasma and then a dilute solution of molecules is spin-deposited on the substrates. The sample is glued to a standard 28 pin chip carrier using silver paint. Electrical connection to the samples is made by an ultrasonic wire bonder using 25 μm Al-Si (1% Si) wires. The chip carrier is mounted in a chip socket in a cryostat afterwards.

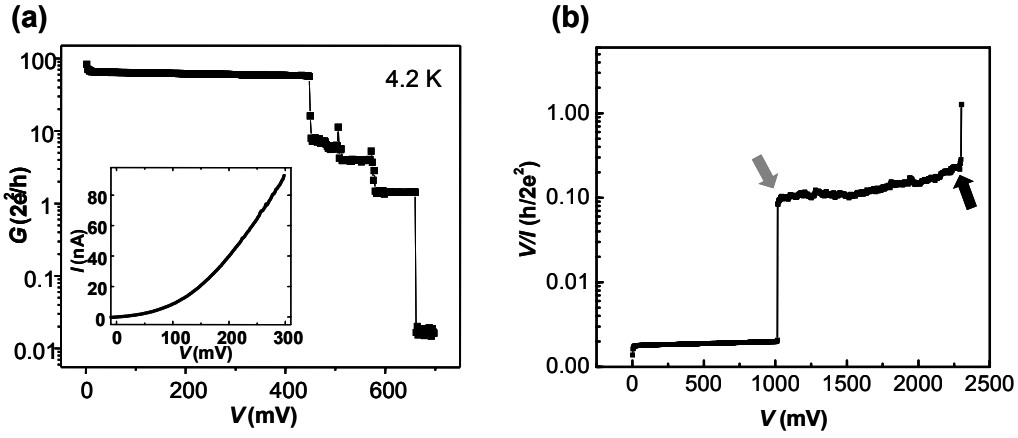

Figure 3.7 Plots of conductance and resistance during electromigration. (a) Breaking condition of bare Au nanowire. Conductance decreases stepwise in quanta conductance. (b) Breaking condition with a resistance tail as typical with devices with molecules deposited.

Figure 3.7 (a) shows a typical breaking curve of a bare Au nanowire. The sample is cooled down to 4.2 K and then Au nanowire is broken via the electromigration process by ramping up a dc voltage across the wire while monitoring the conductance. The preparation is the exactly same as molecular devices except with a clean solvent

containing no molecules. The constriction of the wire is broken stepwise in quantized conductance. This implies that atomic conduction channels are broken up one by one discretely. The inset shows the tunneling current afterwards. This reveals that the created gap is indeed small enough for molecule connection.

For molecular devices, the breaking process is terminated when the resistance across the wires increases above ~100 kΩ. In most devices, the breaking occurs via a series of discrete resistance steps. After breaking, these devices show either simple tunneling current with no gate dependence or no measurable current, suggesting either no molecules are bridging the gaps or the gaps are too large. In some devices, the breaking process is characterized by long resistance tails as illustrated in Fig. 3.7 (b), in which the electromigration starts at around 1 V marked by a grey arrow and the resistance eventually goes to the tunneling regime with value higher than the quantum of resistance h/e^2 marked by a black arrow. The current-voltage (*I*-*V*) characteristics after breaking with a resistance tail more frequently display voltage gaps and current steps which can be modulated with a gate voltage. This means that these devices may potentially be molecule-trapped ones. For these devices, conductance is measured in detail as a function of bias and gate voltages either by using standard ac lock-in technique or by numerically differentiating dc *I*-*V* curves at different gate voltages.

Unexpectedly, we have observed regular Coulomb diamonds sometimes as shown in Fig. 3.8. This is very similar to the experimental results[3] on Au nanoparticles, which are intentionally fabricated by thin Au film deposition, producing Au nanoparticles. First of all, the charging energy is comparable to those in Ref. 3. Second, we have not observed excitation line features around Coulomb diamond in these devices at 4.2 K. Thus, we believe that these Coulomb blockade behaviors are most likely attributed to small Au nanoparticles created by the electromigration itself. It has been pointed out by

other group[5, 6] that artificial metal grains can mimic the transport properties of single-molecule devices. These examples show that experimental data should be interpreted carefully. As we will explain in detail later, we believe that the devices having excitation features can be unambiguously associated with the presence of molecules bridging the nanogaps.

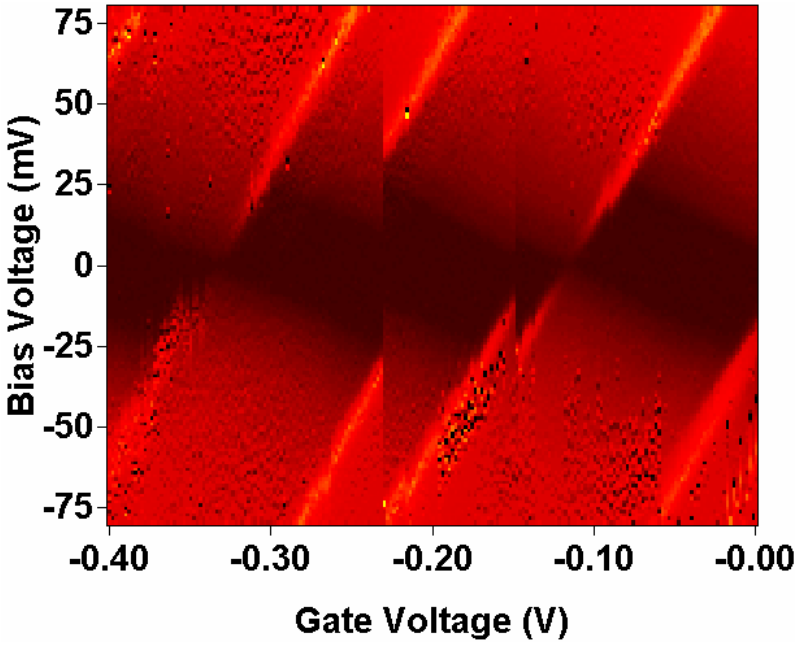

Figure 3.8 Coulomb blockade feature due to a small nanoparticle generated by electromigration.

REFERENCES

[1] H. Park, A. K. L. Lim, A. P. Alivisatos, J. Park, and P. L. McEuen, Appl. Phys. Lett. **75**, 301 (1999).

[2] W. J. Liang, M. P. Shores, M. Bockrath, J. R. Long, and H. Park, Nature **417**, 725 (2002).

[3] K. I. Bolotin, F. Kuemmeth, A. N. Pasupathy, and D. C. Ralph, Appl. Phys. Lett. **84**, 3154 (2004).

[4] G. Lientschnig, PhD thesis, Delft University of Technology (2003).

[5] A. A. Houck, J. Labaziewicz, E. K. Chan, J. A. Folk, and I. L. Chuang, Nano Lett. **5**, 1685 (2005).

[6] H. B. Heersche, Z. de Groot, J. A. Folk, L. P. Kouwenhoven, H. S. J. van der Zant, A. A. Houck, J. Labaziewicz, and I. L. Chuang, Phys. Rev. Lett. **96** (2006).

Chapter 4. Vibrational Excitations in Single Trimetal-Molecule Transistors

4.1 INTRODUCTION

Understanding electron transport through molecules remains one of the challenges in the emerging area of molecular electronics. Recently, individual molecules have been incorporated in a transistor geometry in which the electron transport can be modulated by a gate electrode[1-8]. Transport in these devices at low temperature is dominated by single-electron tunneling[9] or the Coulomb blockade effect, which has provided a new spectroscopic tool to investigate the electronic and vibrational states at the level of individual molecules. These measurements have revealed a number of interesting phenomena including strong coupling of electron transport with molecular vibrational excitations[1, 6, 8] and the Kondo effect[2, 3, 5, 7] due to correlations between unpaired electrons in the molecules and conduction electrons in the electrodes.

Previous measurements so far have focused on conjugated organic molecules or molecules containing only one or two metal atoms. Among other intriguing candidates for molecular electronics are the compounds with linear arrays of metal atoms[10, 11], especially those having extended metal atom chains (EMACs)[12]. Such molecules have also been an important subject in the fundamental research of metal-metal interactions[13-15]. A unique feature of these molecules is that by using appropriate ligands, they can be extended in length with high stability[16]. Moreover, they generally have easily accessible redox states with interesting redox properties. For example, it has been shown that metal-metal separations are strongly dependent on the redox states due to metal-metal bond

This chapter is based on the paper: D. Chae, J. F. Berry, S. Jung, F. A. Cotton, C. A. Murillo, and Z. Yao, Nano Lett. **6**, 165 (2006).

formation in some molecules[14, 15]. This property has led to the proposal to use these molecules as molecular switches.

In this chapter, we report the fabrication and characterization of single-molecule transistors (SMTs) incorporating trinuclear dipyridylamido complexes, $Cu_3(dpa)_4Cl_2$ and $Ni_3(dpa)_4Cl_2$ (dpa = 2,2'-dipyridylamide), which represent the simplest prototypical examples of EMAC molecules. Low-energy excitations are observed in Coulomb blockade tunneling spectroscopy at 4.2 K, which can be attributed to vibrational excitations coupled to the electron tunneling processes. Several charge states can be accessed in the $Cu_3(dpa)_4Cl_2$ molecules by tuning the gate voltage. Vibrational excitations are found to evolve as a function of the charge state of the molecules, which implies a change in the nature of the metal-metal interactions upon reduction or oxidation of the molecules.

4.2 SAMPLE FABRICATION

$Cu_3(dpa)_4Cl_2$ (tricopper) and $Ni_3(dpa)_4Cl_2$ (trinickel) molecules are synthesized according to established procedures[15, 17]. A schematic of our SMTs is shown in Fig. 4.1(a). The devices are fabricated on oxidized silicon substrates. Aluminum gate electrodes are first fabricated by optical lithography and electron-beam evaporation at liquid nitrogen temperature, and subsequently oxidized by exposure to air. Thin gold nanowires with narrow constriction of ~100 nm and thickness of ~15 nm are patterned by electron-beam lithography on top of the aluminum gates, as shown in the atomic force microscope image in Fig. 4.1(b). After the nanowires are cleaned in oxygen plasma, a dilute solution (~0.2 μM) of the trimetal molecules in methanol is spin-deposited on the substrates. The samples are then cooled to 4.2 K and Au nanowires are broken via the electromigration process to create nanometer-sized gaps by ramping up a dc voltage across the wires while monitoring the resistance[18]. The breaking process is terminated

when the resistance across the wires increases above ~100 kΩ. We have examined a total of 160 tricopper and 160 trinickel devices. In most devices, the breaking occurs via a series of discrete resistance steps. After breaking, these devices show either simple tunneling current with no gate dependence or no measurable current, suggesting either no molecules are bridging the gaps or the gaps are too large. In 14 tricopper and 9 trinickel devices, the breaking process is characterized by long resistance tails, and the current-voltage (*I-V*) characteristics after breaking display voltage gaps and current steps which can be modulated with a gate voltage. For these devices, conductance is measured in detail as a function of bias and gate voltages either by using standard ac lock-in technique or by numerically differentiating dc *I-V* curves at different gate voltages. Among these devices, four tricopper and 7 trinickel devices show well-resolved low-energy excitations. As will be explained later, we believe that these devices are associated with the presence of molecules bridging the nanogaps.

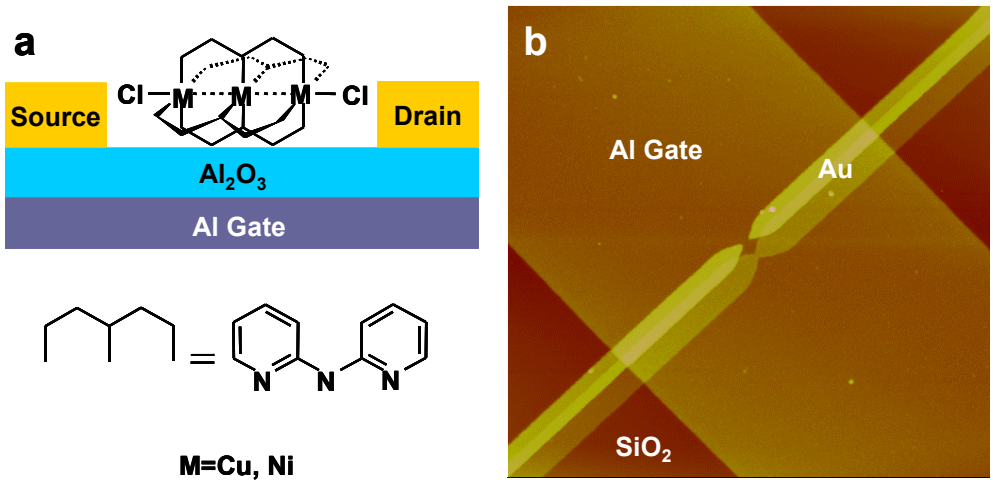

Figure 4.1 Single-trimetal transistor. (a) Schematic of a single trimetal-molecule transistor. (b) An atomic force microscopic image of an Au nanobridge fabricated by electron-beam lithography and double-angle evaporation on top of Al gate electrode with a width of 5 μm.

4.3 EXPERIMETAL RESULTS

Figure 4.2 shows a two-dimensional color plot of differential conductance (d*I*/d*V*) as a function of bias and gate voltages for a SMT incorporating a tricopper molecule. The conductance is suppressed around zero bias and the size of the voltage gaps can be modulated with the application of a gate voltage. Three diamond-shaped regions can be identified in which the conductance is suppressed. There are additional bright lines running parallel to the boundaries of the blockaded regions corresponding to peaks in d*I*/d*V*.

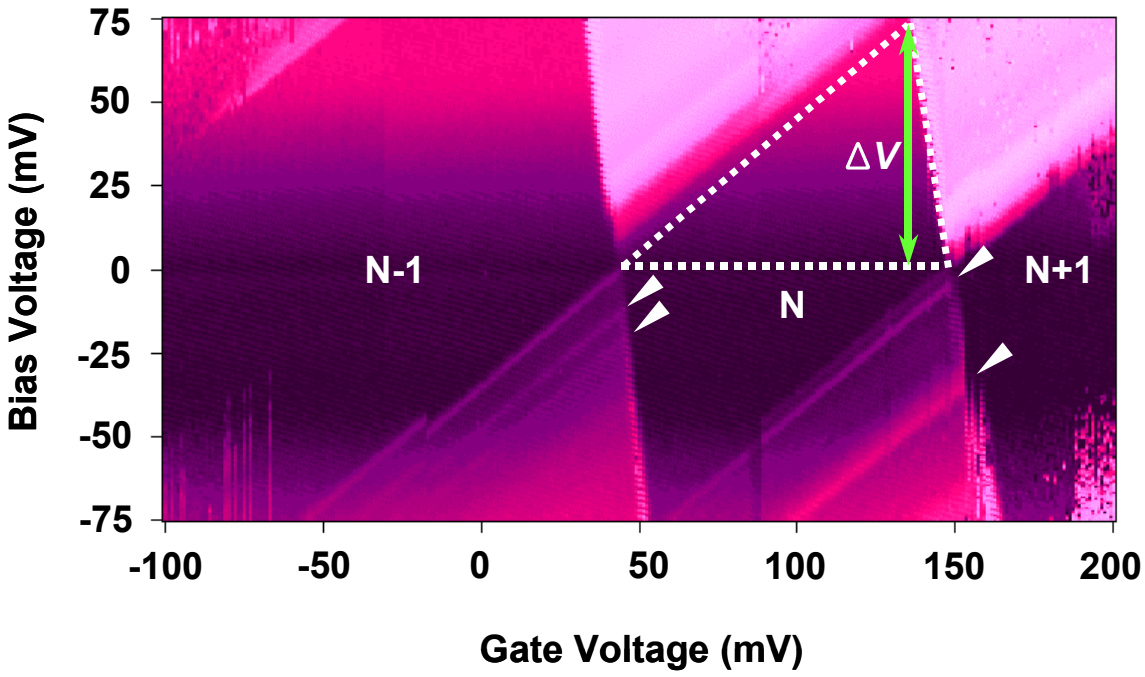

Figure 4.2 Color plot of d*I*/d*V* on logarithmic scale vs. bias and gate voltages for a tri-copper SMT measured at 4.2 K. Bright/dark colors correspond to high/low conductance. The plotted conductance ranges from 10^{-12} to 10^{-8} S. Low-energy excitations at 12.5 mV and 20.5 mV in the N electron state and at 5 mV and 33 mV in the N+1 state are marked by arrows. This is the only device in which more than one charge degeneracy point was accessible.

These features are characteristic of Coulomb blockade or single-electron tunneling behavior, which occurs when the molecule is weakly coupled to the electrodes through tunneling contacts. Similar phenomena have been observed in previous SMT measurements[1-8]. In this transport regime, electrons are added to the molecule one by one as an increasingly positive gate voltage is applied. Each diamond-shaped region corresponds to a distinct redox or charge state of the molecule. The initial charge state of the molecule in the absence of a gate voltage depends on the electrostatic environment and cannot be determined independently. The slopes of the boundaries of blockaded regions are determined by the capacitances of the molecule with respect to the contacts and to the gate. Thus the observation of constant slopes for the three diamonds in Fig. 4.2 indicates that a single molecule is bridging the gap. The voltage ΔV at which the boundaries of Coulomb diamonds intersect is a measure of the addition energy, which includes Coulomb charging energy and molecular energy level spacing. The plot in Fig.4. 2 also provides a mapping of excitation energies in the molecules. A peak in dI/dV occurs whenever an excited state enters the bias voltage window which provides an additional current pathway. The energies of the excited states in a particular charge state are obtained directly from the plot in Fig. 4.2 as the bias voltage values at which the lines associated with the excited states intersect the boundaries of the Coulomb diamond in that charge state. For example, the arrows in the central Coulomb diamond in Fig. 4.2 mark the excited states in the N charge state.

We have consistently observed low-energy excitations in different trimetal SMT devices. Figure 4.3 shows plots of differential conductance from two devices incorporating trinickel molecules. Only one charge degeneracy point was observed in these devices. The exact values of excitations do vary from sample to sample. However,

they are all on the same order of a few tens of mV. In Fig. 4.4, we plot histograms of the excitation energies observed in the 4 tricopper and 7 trinickel devices.

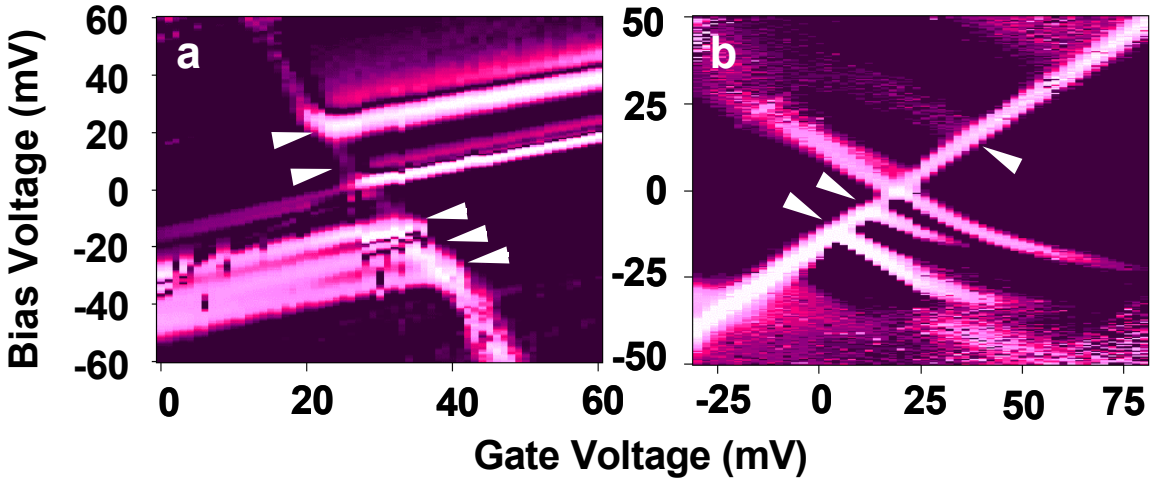

Figure 4.3 Color plots of dI/dV as a function of the bias and gate voltages for two different tri-nickel SMTs measured at 4.2 K. (a) The plotted conductance range from 10^{-10} to 8×10^{-8} S. (b) The plotted conductance range from 10^{-10} to 9×10^{-8} S. Excitations are marked by white arrows.

We note that the observed addition energies of ~ 100 meV in Fig. 4.2 are an order of magnitude smaller than the electronic energy level spacing obtained in solution from conventional spectroscopic measurements of trimetal molecules, which is typically a few eV.[15] However, such a discrepancy was also observed previously in SMTs with conjugated oligomers and was attributed to the screening effect by image charges in the metal electrodes[4]. The addition energies observed in our molecular devices are similar to those exhibited by single-electron transistors based on Au nanoparticles, which were formed by Au evaporation between nanogaps[19]. In those devices, however, all the Coulomb diamonds were of the same sizes and no excited states could be resolved in the tunneling spectroscopy at 4.2 K. We have also performed control experiments in which devices were fabricated in the same way as described above except only pure methanol

was spin-coated on the substrates. Four out of a total of ~60 test devices showed gated transport with addition energies of less than 100 meV, but none of them showed any excitations in *I-V* or dI/dV as in Fig. 4.2 and Fig. 4.3. These devices were presumably due to small Au nanoparticles that were nucleated in the nanogaps during electromigration. Incidentally, formation of gold nanoparticles can probably also account for those molecular devices which did not show excited states. Taking these considerations together, we believe that the data shown in Fig. 4.2 and Fig. 4.3 are indeed associated with the molecules.

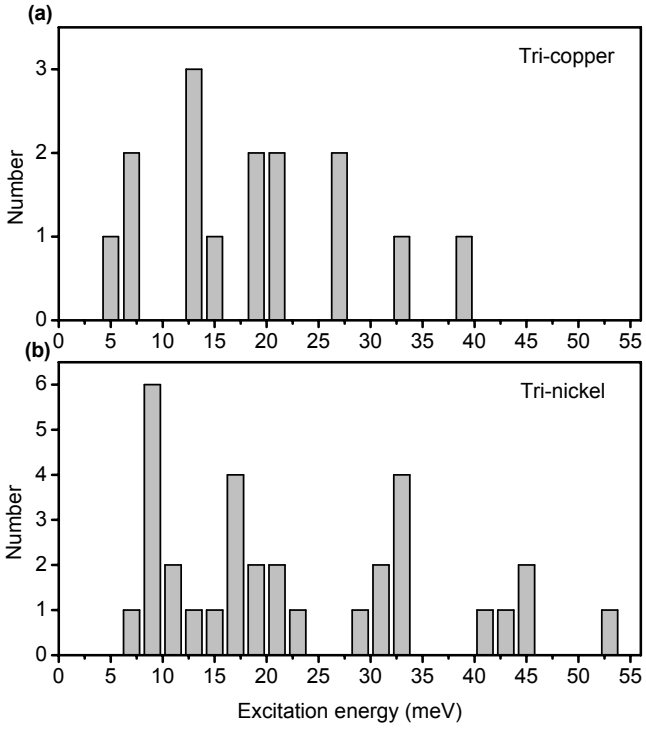

Figure 4.4 Histograms of observed excitations (bin = 2 meV) for trimetal devices. (a) Histogram for tricopper devices. (b) Histogram for trinickel devices.

4.4 DISSCUSSIONS

One common possibility for the excitations observed in Coulomb blockade measurements is electronic excitations. However, excitations of this type are unlikely to be the origin of the excitations observed in the present devices. Within the Coulomb blockade model, the difference in addition energies between adjacent Coulomb diamonds corresponds to the energy level spacing or the difference in energy level spacings. From Fig. 4.2, the difference between the two complete diamonds is more than 50 meV, which is much larger than the 10-20 meV energy values observed in the excitation spectroscopy. Recent SMT measurements have revealed vibrational excitations as a mechanism that can couple to electronic transport.[1, 8] For example, in C_{60} SMTs, ~5 meV excitations were observed consistent with center-of-mass vibrations of the molecules.[1] The molecules in the present work are of similar molecular mass to C_{60} and thus should exhibit similar center-of-mass vibrational energies assuming similar confinement potential. However, the observed excitations are larger. Moreover, if the center-of-mass vibrations are dominant, we should see excitations of similar values in almost every device, which is not the case.

We thus attribute the excitations observed in our SMTs to internal molecular vibrations. The observed excitation energies shown in Fig. 4.4 are in the range of those for metal-metal stretching modes in dinuclear compounds[20] studied by Raman spectroscopy. Other stretching modes such as metal-nitrogen deformations lie at higher energies. It is thus reasonable to assign the observed excitations to the internal stretching modes of the rod-like molecules even though it is probably difficult to separate pure stretches from other vibrational modes because of the complex structure of the molecules. Such modes are also expected to couple to the electron transport more strongly than other modes. To the best of our knowledge, however, internal stretches have not been identified

in the vibrational spectroscopy of trimetal molecules. Nevertheless, to gain some insight into these stretching modes, we can model the trimetal molecules as three effective masses connected by two springs, each having the same effective force constant k (Fig. 4.5(a)). The effective masses are assigned as follows: m_A consists of one copper (nickel) atom, four nitrogen atoms and one third of total carbon and hydrogen atoms and m_B consists of the same atoms together with an additional chlorine atom. In this model, there are two normal stretching modes along the axis: one is the symmetric (in-phase) (Fig. 4.5(b)) and the other is asymmetric (out-of-phase) (Fig. 4.5(c)). The ratio of the energy of the asymmetric mode, E_a, to that of symmetric mode, E_s, is given by: $\frac{E_a}{E_s} = \sqrt{\frac{\mu}{m_B}}$, where $\mu = m_A + 2m_B$ is the total mass of the molecule.[21] In the plot shown in Fig. 4.2, two excitations can be clearly identified for the N electron charge state. If the lower excitation (12.5 meV) is assigned to the symmetric vibrational model, using the expression above, the asymmetric vibrational energy can be estimated to be 22.7 meV, which is indeed close to the observed value, 20.5 meV, for the higher excitation.

When one more electron is added to the tricopper molecule, the excited states change significantly (Fig. 4.2). New excitations at 5 meV and 33 meV appear for the N+1 electron state. Previous studies[15] have shown that upon oxidation or reduction metal-metal separations in trimetal molecules may change because of electrostatic interactions between metal atoms or because of formation of metal-metal bonds. The new excitations can be accounted for if we assume the two effective force constants between metal atoms become asymmetric. However, one cannot rule out the possibility that other vibrational modes are involved such as metal-ligand stretching, bending or twisting deformations. A more realistic theoretical model is required in order to determine which modes couple to the electron tunneling processes most effectively.

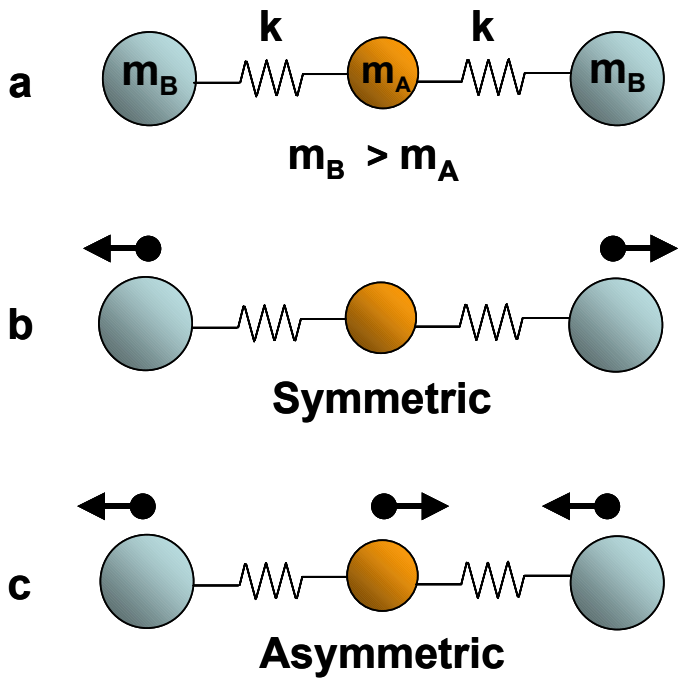

Figure 4.5 Toy model for the vibrational modes of trimetal molecule. (a) Schematic of mass-spring model for the trimetal molecules. (b) Symmetric stretching mode. (c) Asymmetric stretching mode.

4.5 SUMMARY

In summary, we have fabricated SMTs incorporating trimetal EMAC complexes and observed single-electron tunneling through the molecules. Low-energy excitations have been consistently observed in the tunneling spectroscopy. These features can be attributed to intramolecular stretching excitations, consistent with our simple analysis based on a mass and spring model. Furthermore, the observed vibrational excitations evolve when the charge state of the molecule is changed, highlighting the effect of metal-metal interactions upon reduction and oxidation of these compounds.

REFERENCES

[1] H. Park, J. Park, A. K. L. Lim, E. H. Anderson, A. P. Alivisatos, and P. L. McEuen, Nature **407**, 57 (2000).

[2] W. J. Liang, M. P. Shores, M. Bockrath, J. R. Long, and H. Park, Nature **417**, 725 (2002).

[3] J. Park, A. N. Pasupathy, J. I. Goldsmith, C. Chang, Y. Yaish, J. R. Petta, M. Rinkoski, J. P. Sethna, H. D. Abruna, P. L. McEuen, and D. C. Ralph, Nature **417**, 722 (2002).

[4] S. Kubatkin, A. Danilov, M. Hjort, J. Cornil, J. L. Bredas, N. Stuhr-Hansen, P. Hedegard, and T. Bjornholm, Nature **425**, 698 (2003).

[5] A. N. Pasupathy, R. C. Bialczak, J. Martinek, J. E. Grose, L. A. K. Donev, P. L. McEuen, and D. C. Ralph, Science **306**, 86 (2004).

[6] L. H. Yu, Z. K. Keane, J. W. Ciszek, L. Cheng, M. P. Stewart, J. M. Tour, and D. Natelson, Phys. Rev. Lett. **93** (2004).

[7] L. H. Yu and D. Natelson, Nano Lett. **4**, 79 (2004).

[8] A. N. Pasupathy, J. Park, C. Chang, A. V. Soldatov, S. Lebedkin, R. C. Bialczak, J. E. Grose, L. A. K. Donev, J. P. Sethna, D. C. Ralph, and P. L. McEuen, Nano Lett. **5**, 203 (2005).

[9] L. P. Kouwenhoven, C. M. Marcus, P. L. McEuen, S. Tarucha, R. M. Westervelt, and N. S. Wintergreen, in *Mesoscopic Electron Transport*, edited by L. P. Kouwenhoven, G. Schon and L. L. Sohn (Kluwer Academic Publishers, Dordrecht, The Netherlands, 1996).

[10] J. K. Bera and K. R. Dunbar, Angew. Chem., Int. Ed. **41**, 4453 (2002).

[11] C. R. Kagan and M. A. Ratner, MRS Bull. **29**, 376 (2004).

[12] J. F. Berry, in *Multiple Bonds between Metal Atoms*, edited by F. A. Cotton, C. A. Murillo and R. A. Walton (Springer, New York, 2005).

[13] J. F. Berry, F. A. Cotton, L. M. Daniels, and C. A. Murillo, J. Am. Chem. Soc. **124**, 3212 (2002).

[14] C. Y. Yeh, C. H. Chou, K. C. Pan, C. C. Wang, G. H. Lee, Y. O. Su, and S. M. Peng, J. Chem. Soc., Dalton Trans., 2670 (2002).

[15] J. F. Berry, F. A. Cotton, L. M. Daniels, C. A. Murillo, and X. P. Wang, Inorg. Chem. **42**, 2418 (2003).

[16] J. F. Berry, F. A. Cotton, P. Lei, T. Lu, and C. A. Murillo, Inorg. Chem. **42**, 3534 (2003).

[17] J. F. Berry, F. A. Cotton, P. Lei, and C. A. Murillo, Inorg. Chem. **42**, 377 (2003).

[18] H. Park, A. K. L. Lim, A. P. Alivisatos, J. Park, and P. L. McEuen, Appl. Phys. Lett. **75**, 301 (1999).

[19] K. I. Bolotin, F. Kuemmeth, A. N. Pasupathy, and D. C. Ralph, Appl. Phys. Lett. **84**, 3154 (2004).

[20] D. F. Shriver and C. B. Cooper, in *Advances in Infrared and Raman Spectroscopy*, edited by R. J. H. Clark and R. E. Hester (John Wiley, New York, 1979), Vol. 6.

[21] L. D. Landau and E. M. Lifshitz, *Mechanics* (Pergamon Press, New York, 1976).

Chapter 5. Higher-Order Tunneling Processes in Single-Molecule Transistors

5.1 INTRODUCTION

Recently, electron transport experiments through individual molecules have been carried out extensively using electromigration technique[1]. This approach enables a nearby gate, which is of importance to manipulate the charge state of inserted molecule while the transport properties are investigated in single-molecule devices. Several early experiments[2-6] have demonstrated that the transport is strongly affected by the electron-vibration interactions in the single-molecule transistors (SMTs) in the single-electron tunneling regime[7]. Furthermore, it has been reported that the electron transport is appreciable even in the Coulomb blockade region due to cotunneling processes via vibrational degrees of freedom in single-molecule transistors[5]. The tunability of charge state of individual molecules has also allowed the study of the electronic structure of a redox-active molecule[8]. Moreover, it has been shown that the transport is significantly influenced by the spin degree of freedom through the Kondo effect[9] resulting from a strong exchange entanglement between spins in the inserted molecules and conduction electrons in the electrodes[4, 5, 10-14]. More recently, an experimental study[13] on the evolution of the Kondo resonances with respect to the electron number of the molecules suggests that the transport measurement might be utilized to assign spin configurations of individual molecules in different charge (redox) states.

In this work, we use Co-porphyrin and cyclo[6]pyrrole, one of synthesized expanded prophyrins, to fabricate SMTs with the following motivations. Co-porphyrin is one species of metalloporphyrins, which are of importance in biological systems including photosynthetic units in plant and heme proteins in blood[15]. Co-porphyrin

consists of Co ion at the center and a cage ligand having 18 π electrons as illustrated in Fig. 5.1 (a). It is experimentally reported that Co^{2+} (neutral charge state) and Co^{3+} (oxidized charge state) are most stable in solution even though Co^{+} state could be possible[16]. According to previous optical and resonance Raman spectroscopic characterizations, electronic structures and intramolecular vibrations are strongly dependent on the redox state[17]. Co-porphyrin is thus expected to be an intriguing system to be investigated with respect to redox state at the single molecule level. Cyclo[6]pyrrole is another interesting compound having 22 π electrons[18]. Electrochemical studies indicate that the energy gap between the highest occupied molecular orbital and the lowest unoccupied molecular orbital of cyclo[6]pyrrole is smaller than that of porphyrins[18]. Consequently, the redox states of cyclo[6]pyrrole are more easily accessible compared to the ordinary porphyrins. It is known that cyclo[6]pyrrole has two reduction states and two oxidation states while Co-porphyrin has two accessible charge states[18]. Thus, it is envisioned that cyclo[6]pyrrole is also an interesting candidate for the study of transport properties resulting from the redox processes.

We have observed interesting transport phenomena including cotunneling, the Kondo effect, and exotic low-energy gaps even at degeneracy points. Cotunneling features are similar to the results in Ref. 6 and the Kondo effect is consistent with the previous observations[5, 10, 11, 14] in other SMTs whereas the energy gap features have not been reported yet. The sample preparation is described first and the experimental results and discussions follow.

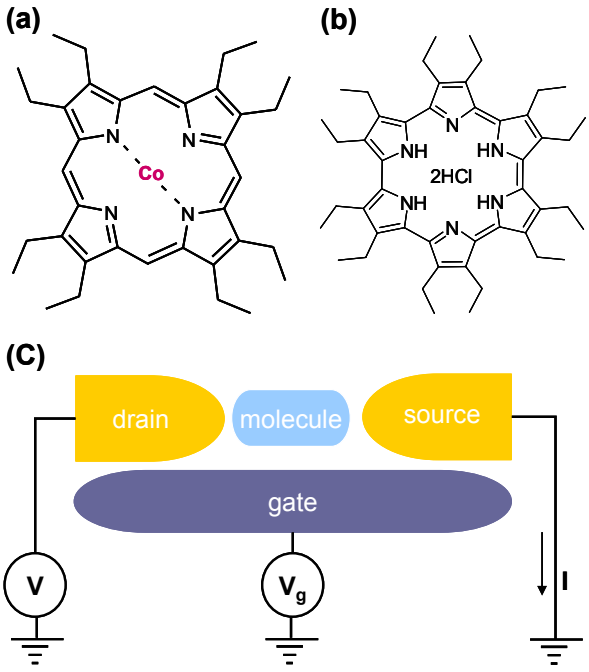

Figure 5.1 Single-porphyrin transistor. (a) Structure of Co-porphyrin. (b) Structure of cyclo[6]pyrrole. (c) Schematic diagram of single-molecule transistor.

5.2 SAMPLE PREPARATION

A schematic diagram of a device incorporating Co-porphyrin (Fig. 5.1 (a)) and cyclo[6]pyrrole (Fig. 5.1 (b)) is shown in Fig. 5.1 (c). A dilute (~0.2 μM) solution of Co-porphyrin or cyclo[6]pyrrole in dicholomethane is spin-deposited on Au nanowires, which are fabricated by electron-beam lithography. The electromigration is performed subsequently in order to trap molecules in nanometer-sized gaps in-situ as described in Chapter 3. 13 out of 91 Co-porphyrin- and 28 out of 260 cyclo[6]pyrrole-devices show the Coulomb blockade behavior with strong gate modulation. For these devices, we measure conductance in detail as a function of bias and gate voltages by numerically

differentiating dc current-voltage curves or by using ac lock-in technique at different gate voltages.

5.3 EXPERIMETAL RESULTS OF HIGHER-ORDER TUNNELING PROCESSES

Figure 5.2 (a) shows a two-dimensional color plot of differential conductance ($\partial I/\partial V$) as a function of bias and gate voltages for a Co-porphyrin device at 4.2 K. The plot shows some generic features of Coulomb blockade: the conductance is suppressed within the Coulomb diamonds and low-energy excitations (24±1 meV and 39±1 meV) are aligned parallel to the boundaries of the diamond-shaped regions. Interestingly, we observe a horizontal line feature (marked by two white arrows) parallel to the gate axis within the blockade zone. The boundary line is connected to the low-energy excitation at 39±1 meV. When the applied bias is larger than ~39 meV, the conductance value is rather high even in the blockade region. This phenomenon can be understood in term of the inelastic cotunneling process in which two or more electrons are involved in tunneling via a low-energy excitation as explained in Chapter 2. Figure 5.2 (b) illustrates $\partial^2 I/\partial V^2$ as a function of bias and gate voltages for another Co-porphyrin device at 4.2 K. Conductance values, which are measured by an ac lock-in technique with an excitation voltage of 0.3 mV at 7 Hz, are differentiated to show the horizontal parallel line features within the blockade zone more clearly. Two horizontal lines are connected to two low-energy excitations (31±2 meV and 52±2 meV) at the edge of the Coulomb diamond. We note that unlike Fig. 5.2 (a), the two horizontal lines are manifested as peaks along the bias voltage because the conductance is differentiated. The observed low-energy excitations in Fig. 5.2 (a) and (b) are in the range of vibrational modes of metalloporphyrins based on normal-coordinate analyses[19, 20]. However, a precise assignment is not trivial since local environments may greatly affect the values.

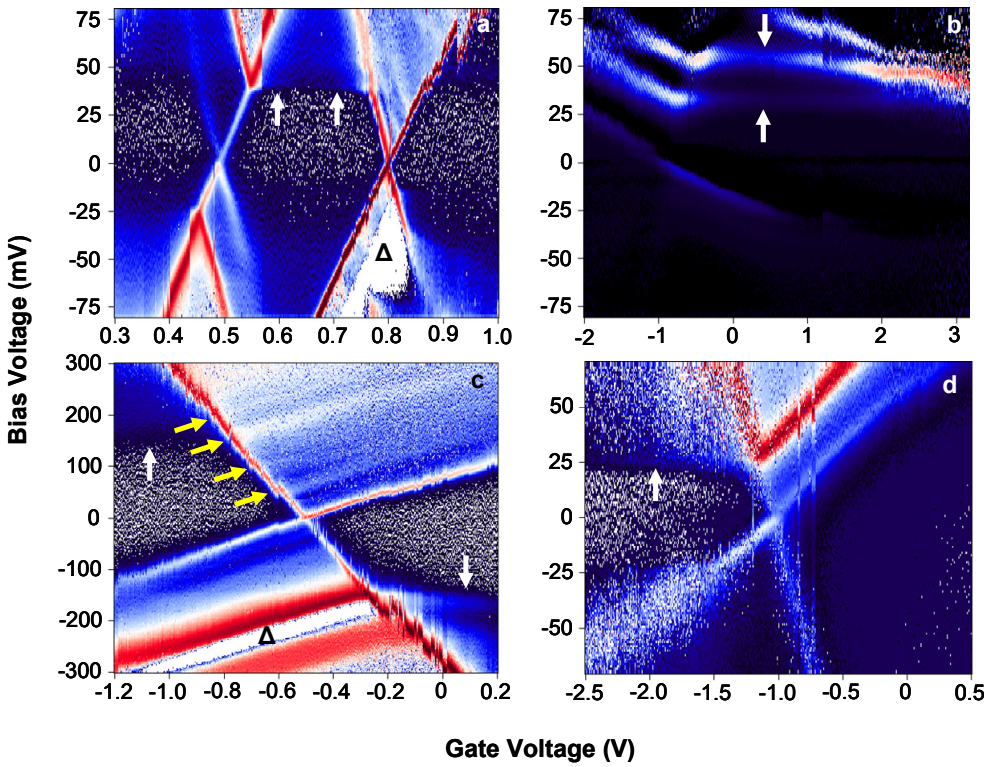

Figure 5.2 Cotunneling processes. (a) Color plot of $\partial I / \partial V$ vs. bias and gate voltages for Co-porphyrin SMT. (b) $\partial^2 I / \partial V^2$ vs. bias and gate voltages for Co-porphyrin device. (c) $\partial I / \partial V$ vs. bias and gate voltages for cyclo[6]pyrrole SMT device. (d) $\partial I / \partial V$ vs. bias and gate voltages for cyclo[6]pyrrole SMT device. The plots are on logarithmic scale with the range from 10^{-11} to 10^{-7} S for (a),(c) and (d).

Figure 5.2 (c) and (d) illustrate similar cotunneling features within the blockade regions in two cyclo[6]pyrrole devices. Intriguingly, Figure 5.2 (c) shows the harmonics of a fundamental excitation of around 50 meV as marked with yellow arrows. This is a strong evidence that the excitations result from the intramolecular vibrational excitations of the inserted molecule. In addition, the horizontal boundary line of the cotunneling

feature is aligned with the third harmonic at about 150 meV. It implies that the cotunneling arises via a quantized state of vibrational excitation and not via an electronic state as in a quantum dot[21]. However, precise identification of vibrational excitations is difficult since cyclo[6]pyrrole is recently synthesized and thus the vibrational excitations of this compound have not been characterized. In addition, since the local electrostatic environment may significantly affect the characteristic internal vibrational modes, the observed excitations may be different from those of isolated molecules. The white regions in the conductance plots in Fig. 5.2 (a) and (c) marked by Δ correspond to negative differential conductance values. Detailed understanding of these features in our devices is still lacking at this moment.

We now turn to another interesting feature, i.e., zero-bias resonances (ZBRs), taken from Co-porphyrin SMTs. Figure 5.3 displays color plots of differential conductance as a function of bias and gate voltages for four different Co-porphyrin devices (Device A to D corresponding Fig. 5.3 (a) to Fig. 5.3 (d)). All four devices display characteristic features of the Coulomb blockade effect. In addition, ZBRs are reproducibly observed. By adding (subtracting) one electron to (from) the trapped molecule with a gate voltage, the presense of ZBR is controlled with the parity of the electron number. We usually observe one degeneracy point within our available gate range (about -3 to 3 V). It means that two electron charge states are accessible in most devices. Only Device C shows two degeneracy points. That is, three charge states are accessible in the inserted Co-porphyrin.

In order to investigate the origin of ZBRs, we have carried out the temperature and magnetic field dependence measurements for Device C and Device D, respectively. Figure 5.4 (a) shows the temperature dependence of differential conductance for Device C, measured with ac lock-in technique (0.3 mV as an excitation voltage at 7 Hz) at zero

gate voltage. The peak conductance decreases as the temperature increases. The inset of Fig. 5.4 (a) presents the logarithmic dependence of the ZBR with respect to temperature. Figure 5.4 (b) shows the Zeeman splitting of the ZBR in Device D shown in Fig. 5.3 (d)

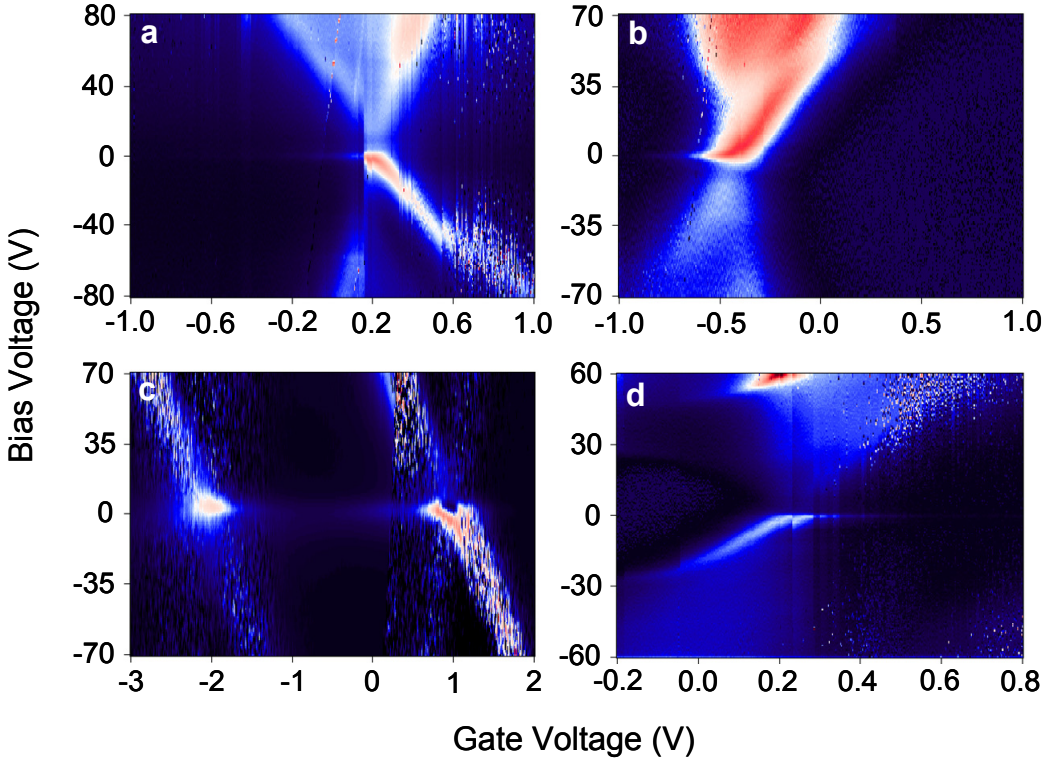

Figure 5.3 The Kondo resonances in Co-porphyrin SMTs. Color plots of $\partial I / \partial V$ as a function of the bias and gate voltages for four different Co-porphyrin devices. The plotted conductance ranges as follows: (a) from 0 to 2×10^{-8} S. (b) from 0 to 8×10^{-8} S. (c) from 0 to 1×10^{-6} S. (d) from 0 to 1×10^{-9} S.

in an 8 T external magnetic field at 400 mK. These two experimental results indeed confirm that the ZBRs can be attributed to the Kondo effect as described in Chapter 2. We can estimate the Lande g factor from the Zeeman splitting using the relation[22] that the magnitude of the splitting is equal to $2g\mu_B B / e$, where μ_B is the Bohr magneton and B is

the external magnetic field. The magnitude of the splitting is about 2 mV as shown in Fig. 5.4 (b). Thus, the estimated g value is about 2, which is comparable to that of a Co complex reported by Ralph group at Cornell University[11]. In addition, ZBRs have very strong gate dependence. The feature of ZBRs fades out as the gate voltage is adjusted from degeneracy points to blockade regions as shown in Fig. 5.3. This behavior is also consistent with the Kondo effect. That is, the Kondo temperature decays exponentially as a function of "distance" between the energy level and the Fermi energy of electrodes, which can be controlled by the gate voltage, as described in Chapter 2[23, 24]. The Kondo temperature is, on the other hand, proportional to the full width of half maximum (FWHM)[24]. Therefore, this leads to the decrease of FWHM of the Kondo resonance as the gate voltage is tuned away from degeneracy points in conductance plots.

We can assign the spin state of each charged state showing the Kondo behavior based on the reported results[11, 25, 26]. An earlier transport study[11] through single molecules containing Co ion at the center has shown that Co^{2+} ($3d^7$) state has odd number of electrons with the total spin of S=1/2 while Co^{3+} ($3d^6$) state has even number of electrons with S=0. This assignment is consistent with previous studies[25, 26] on magnetic compounds. The binding between the metal ion and the ligands can give rise to the large enough splitting of *d* orbitals to overcome Hund's rule, in which electrons prefer parallel spins in different orbitals. For large enough splitting the higher levels are destabilized, leading to the quenching of magnetic moments of metal ions. Co ionic states in Co-porphyrin are also most stable in Co^{2+} and Co^{3+} in aqueous media according to electrochemical studies[16]. Thus, we can assign the Co^{2+}/Co^{3+} state to the Kondo/non-Kondo resonance in Co-porphyrin devices. For instance, the Co ionic state for Device C in Fig. 5.3 (c) can be assigned to Co^{3+}, Co^{2+}, and Co^{+} for the left Coulomb diamond, the central Coulomb diamond, and the right Coulomb diamond, respectively.

The present experimental observations of the Kondo effect are similar to previous reports[5, 10, 11, 14] on SMTs containing metal ions. The Kondo temperature turns out to be very high in our devices. We can extract the Kondo temperature, T_K, by applying the simple relation[24] that the FWHM of the ZBR is approximately equal to $2k_B T_K / e$. For instance, the estimated Kondo temperature for the Kondo resonance at zero gate voltage in Fig. 5.4 (a) is about 100 K. This indicates that the exchange interaction between the local spin in molecule and the spins of the conduction electrons in electrodes is very strong. This high Kondo temperature is consistent with earlier results[4, 5, 10, 11, 14].

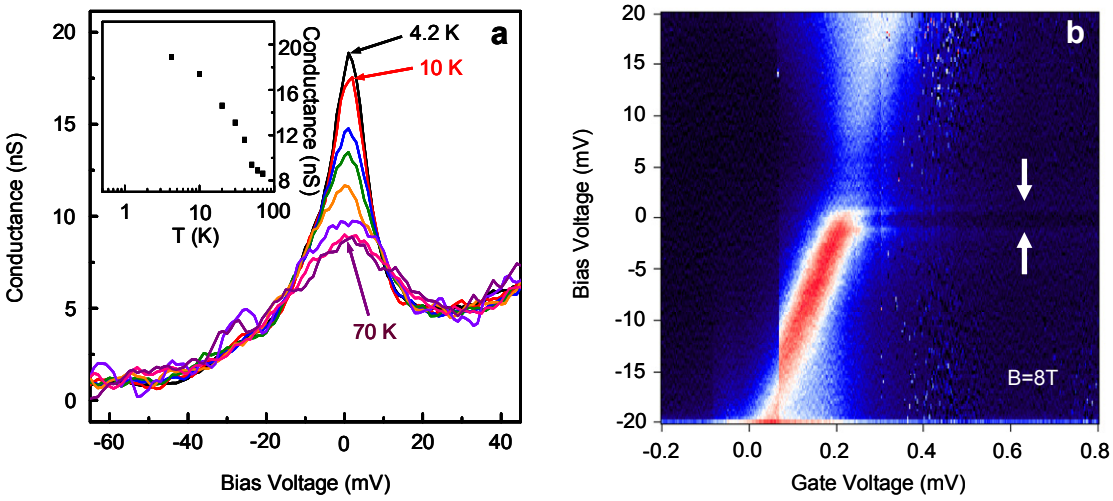

Figure 5.4 Temperature and magnetic field dependences of zero-bias resonances. (a) Temperature dependence of ZBR in Device C at zero gate voltage measured from 4.2 K to 70 K; The temperature increases from 10 K to 70 K in 10 K increments. The inset shows the logarithmic temperature dependence of peak height. (b) Splitting of ZBR (~2 meV) in Device D under an applied magnetic field of 8 T at 400 mK. Two arrows indicate the Zeeman splitting.

Interestingly, most our devices consistently show Kondo resonances at low conductance values. The intensities of the Kondo resonances are usually observed

between 10^{-9} S and 10^{-6} S. In general, the Kondo effect arises from strongly correlated entanglement between the local spins in the island and the spins of conduction electrons in the electrodes through rather transparent tunnel barriers unlike the Coulomb blockade effect observed in weakly tunnel-coupled quantum dots. It is known that the conductance values can reach the unitary value ($2e^2 / h$) for a symmetrically coupled quantum dot[24, 27]. However, our devices have only several to several tens percent of the quantum conductance in contrast to the high conductance values in single-molecule devices reported by other groups[4, 5, 10, 11, 14]. One trivial scenario might be asymmetric coupling of the molecules to the leads. However, it is challenging to prove that scenario experimentally because the tunneling contacts in our devices cannot be adjustable like in a semiconducting quantum dot confined by gate electrodes. We think that other interpretations are still possible. For instance, a recent theoretical work[28] points out a possibility that the electron-vibration interaction in SMT might give rise to the Kondo effect in the low conducting regime.

5.3 LOW-ENERGY GAPS IN TUNNELING SPECTROSCOPY

Remarkably, one of the cyclo[6]pyrrole devices shows low-energy gaps even at the degeneracy points, at which high conductance values should appear according to the Coulomb blockade effect (Fig 5.5 (a)). The conductance value can be recovered by increasing the temperature as shown in Fig. 5.5 (b) and (c). Figure 5.5 (d) shows the temperature dependence of the conductance with respect to gate voltage at zero bias. The conductance value increases with the elevation of temperature, which is opposite to the typical single-electron tunneling behavior of a quantum dot. Recently, J. Koch and his collaborators[29, 30] have theoretically predicted a suppression of conductance owing to strong electron-vibration coupling in SMT, which they termed the Franck-Condon

blockade effect. Similar phenomenon has been observed experimentally in a suspended quantum dot system[31]. It is suggested that the tunneling of an electron onto a molecule triggers the emission of a quantized vibrational excitation for a strong electron-vibration coupled system, leading to the mismatch of the resonance condition as illustrated in Fig. 5.5 (f). This mechanism results in the energy gap even at the degeneracy point as shown in the lower schematic in Fig. 5.5 (f) while the resonance condition is maintained for a weak electron-vibration coupling as illustrated in Fig. 5.5 (e). Our observation seems to be considered with the Franck-Condon blockade effect. We also notice that the blockade is lifted by the thermal broadening of Fermi distribution function. The energy gap approximately corresponds to four times the temperature ($\varepsilon \approx 4k_{\mathrm{B}}T$), consistent with the scenario of the Franck-Condon blockade. However, this is the only sample showing this exotic feature. We believe that if the observation originates from the Franck-Condon blockade, it should be observed more frequently in other devices with the same molecules. We do not fully understand what parameters are crucial to give rise to these low-energy gaps at this moment.

5.5 SUMMARY

In summary, we have observed the cotunneling feature and the Kondo effect in single-electron transistors incorporating Co-porphyrins and cyclo[6]pyrroles. We suggest that the cotunneling arises via the intramolecular vibrational excitations of the inserted molecules. The consistent observation of the Kondo resonance in the very low conductance regime is distinct from previous reports. Moreover, an exotic low-energy gap feature is observed in a cyclo[6]pyrrole device, but its origin is not fully understood.

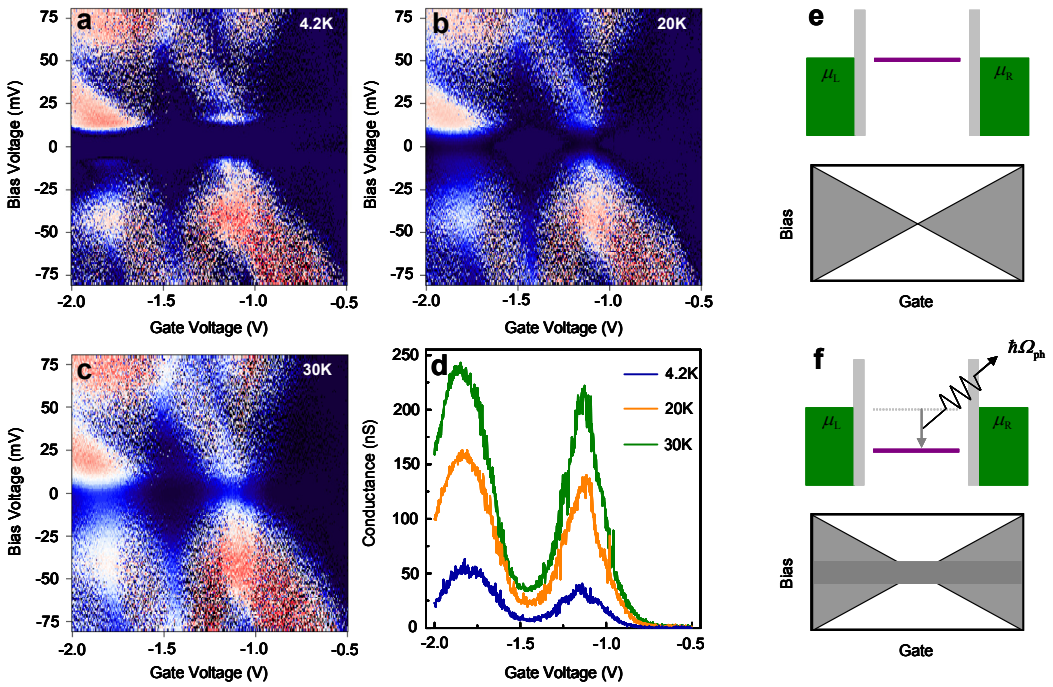

Figure 5.5 Low-energy gaps in a single-cyclo[6]pyrrole transistor.

REFERENCES

[1] H. Park, A. K. L. Lim, A. P. Alivisatos, J. Park, and P. L. McEuen, Appl. Phys. Lett. **75**, 301 (1999).

[2] H. Park, J. Park, A. K. L. Lim, E. H. Anderson, A. P. Alivisatos, and P. L. McEuen, Nature **407**, 57 (2000).

[3] A. N. Pasupathy, J. Park, C. Chang, A. V. Soldatov, S. Lebedkin, R. C. Bialczak, J. E. Grose, L. A. K. Donev, J. P. Sethna, D. C. Ralph, and P. L. McEuen, Nano Lett. **5**, 203 (2005).

[4] L. H. Yu and D. Natelson, Nano Lett. **4**, 79 (2004).

[5] L. H. Yu, Z. K. Keane, J. W. Ciszek, L. Cheng, M. P. Stewart, J. M. Tour, and D. Natelson, Phys. Rev. Lett. **93**, 266802 (2004).

[6] D. Chae, J. F. Berry, S. Jung, F. A. Cotton, C. A. Murillo, and Z. Yao, Nano Lett. **6**, 165 (2006).

[7] L. P. Kouwenhoven, C. M. Marcus, P. L. McEuen, S. Tarucha, R. M. Westervelt, and N. S. Wintergreen, in *Mesoscopic Electron Transport*, edited by L. P. Kouwenhoven, G. Schon and L. L. Sohn (Kluwer Academic Publishers, Dordrecht, The Netherlands, 1996).

[8] S. Kubatkin, A. Danilov, M. Hjort, J. Cornil, J. L. Bredas, N. Stuhr-Hansen, P. Hedegard, and T. Bjornholm, Nature **425**, 698 (2003).

[9] L. P. Kouwenhoven and L. I. Glazman, Physics World **14**, 33 (2001).

[10] W. J. Liang, M. P. Shores, M. Bockrath, J. R. Long, and H. Park, Nature **417**, 725 (2002).

[11] J. Park, A. N. Pasupathy, J. I. Goldsmith, C. Chang, Y. Yaish, J. R. Petta, M. Rinkoski, J. P. Sethna, H. D. Abruna, P. L. McEuen, and D. C. Ralph, Nature **417**, 722 (2002).

[12] A. N. Pasupathy, R. C. Bialczak, J. Martinek, J. E. Grose, L. A. K. Donev, P. L. McEuen, and D. C. Ralph, Science **306**, 86 (2004).

[13] D. Chae, J. Lee, J. L. Sessler, and Z. Yao, In preparation (2006).

[14] L. H. Yu, Z. K. Keane, J. W. Ciszek, L. Cheng, J. M. Tour, T. Baruah, M. R. Pederson, and D. Natelson, Phys. Rev. Lett. **95**, 256803 (2005).

[15] D. Dolphin, *The Porphyrins* (Academic, New York, 1978).

[16] J. Fuhrhop, K. Kadiah, and G. Davis, J. Am. Chem. Soc. **95**, 5140 (1973).

[17] W. A. Oertling, A. Salehi, Y. C. Chung, G. E. Leroi, C. K. Chang, and G. T. Babcock, J. Phys. Chem. **91**, 5887 (1987).

[18] T. Kohler, D. Seidel, V. Lynch, F. O. Arp, Z. P. Ou, K. M. Kadish, and J. L. Sessler, J. Am. Chem. Soc. **125**, 6872 (2003).

[19] X. Y. Li, R. S. Czernuszewicz, J. R. Kincaid, Y. O. Su, and T. G. Spiro, J. Phys. Chem. **94**, 31 (1990).

[20] M. Abe, T. Kitagawa, and Y. Kyogoku, J. Chem. Phys. **69**, 4526 (1978).

[21] S. De Franceschi, S. Sasaki, J. M. Elzerman, W. G. van der Wiel, S. Tarucha, and L. P. Kouwenhoven, Phys. Rev. Lett. **86**, 878 (2001).

[22] Y. Meir, N. S. Wingreen, and P. A. Lee, Phys. Rev. Lett. **26**, 2601 (1993).

[23] N. E. Bickers, Rev. Mod. Phys. **59**, 845 (1987).

[24] W. G. van der Wiel, S. De Franceschi, T. Fujisawa, J. M. Elzerman, S. Tarucha, and L. P. Kouwenhoven, Science **289**, 2105 (2000).

[25] D. A. van Leeuwen, J. M. van Ruitenbeek, L. J. Dejongh, A. Ceriotti, G. Pacchioni, O. D. Haberlen, and N. Rosch, Phys. Rev. Lett. **73**, 1432 (1994).

[26] H. Oshio, H. Spiering, V. Ksenofontov, F. Renz, and P. Gutlich, Inorg. Chem. **40**, 1143 (2001).

[27] T. K. Ng and P. A. Lee, Phys. Rev. Lett. **61**, 1768 (1988).

[28] P. S. Cornaglia, H. Ness, and D. R. Grempel, Phys. Rev. Lett. **93**, 147201 (2004).

[29] J. Koch and F. von Oppen, Phys. Rev. Lett. **94**, 206804 (2005).

[30] J. Koch, F. von Oppen, and A. V. Andreev, cond-mat/0606512 (2006).

[31] E. M. Weig, R. H. Blick, T. Brandes, J. Kirschbaum, W. Wegscheider, M. Bichler, and J. P. Kotthaus, Phys. Rev. Lett. **92**, 046804 (2004).

Chapter 6. Absence of Even-Odd Effect in the Kondo Resonance in Single-Molecule Transistors

6.1 INTRODUCTION

The charge quantization of an electron and the repulsive on-site Coulomb interaction give rise to the single-electron tunneling behavior[1] in three-terminal nanoelectronic devices consisting of a small island connected to source and drain electrodes through tunnel barriers and a nearby gate electrode. When the charging energy exceeds the thermal energy, electron tunneling occurs one by one. At the same time, the spin degree of freedom of an electron also plays a crucial role in the electrical transport. One of the well-understood spin-dependent phenomena is the Kondo effect[2] that arises from the entanglement between a localized spin and delocalized conduction electrons in the reservoir. The Kondo effect leads to an enhancement in the conductance at zero bias in single-electron transistors (SETs) while the same effect suppresses conductance in a conventional metallic system containing magnetic impurities.

The SET allows us to investigate the Kondo effect in more controllable way compared to the conventional system. Since the number of electrons in a SET can be changed by a gate, the Kondo/no-Kondo resonances can generally be manipulated by controlling the odd/even number of electrons, respectively. The Kondo effect has been studied in various SETs, including semiconductor quantum dots,[3, 4] carbon nanotubes,[5-9] and single molecules[10-15]. Recent studies of the Kondo effect in the single-molecule transistors (SMTs) can be categorized by two types of molecules: One class is a molecule containing transition metals at center[10, 11, 13, 14] and the other is a metal-free system such as C_{60}[12, 15]. Molecules studied in this work belong to the latter class.

In this work, cyclo[6]pyrrole[16] (Fig. 6.1(a)) and cyclo[8]pyrrole[17] (Fig. 6.1(b)) have been used to fabricate single-molecule transistors. Cyclo[6]pyrrole is a 22-π-

electron aromatic system and cyclo[8]pyrrole is a 30-π-electron aromatic system. These cyclo[*n*]pyrroles may be considered as larger analogues of porphyrin, in that they are flat, symmetrical and aromatic. However, unlike porphyrins, cyclo[*n*]pyrroles can have multiple oxidation states. Electrochemical studies of cyclo[*n*]pyrroles indicate that the energy gap between the highest occupied molecular orbital (HOMO) and the lowest unoccupied molecular orbital (LUMO) is smaller than that of porphyrins, and that as the size of the expanded porphyrin increases, the HOMO-LUMO separation decreases[16]. One of the interesting features in the electrochemical studies of cyclo[*n*]pyrroles is that they undergo a two-electron reduction process at room temperature. But at low temperature (-78 ºC), the two-electron reduction process can be resolved as two successive one-electron processes. Theoretical calculation predicts that these expanded porphyrins have a degenerate HOMO and a split LUMO pair, which is confirmed by magnetic circular dichroism[18]. Due to these unique characteristics of cyclo[*n*]pyrroles, it is envisioned that they are excellent candidates to investigate the redox chemistry in solid state at the individual molecule level.

Remarkably, we have observed the Kondo resonance peaks appearing for both even- and odd- charge states in single expanded porphyrin transistors. This behavior cannot be described by the conventional spin ½ Kondo effect based on the Anderson impurity model. We suggest a simple model to understand our observations: when the exchange interaction within a molecule is larger than the energy level spacing in the molecule, two successive electrons of the same spin may be added instead of alternating filling of spin-up and spin-down electrons. This leads to the absence of the parity effect in the Kondo resonance in the two consecutive Coulomb diamonds.

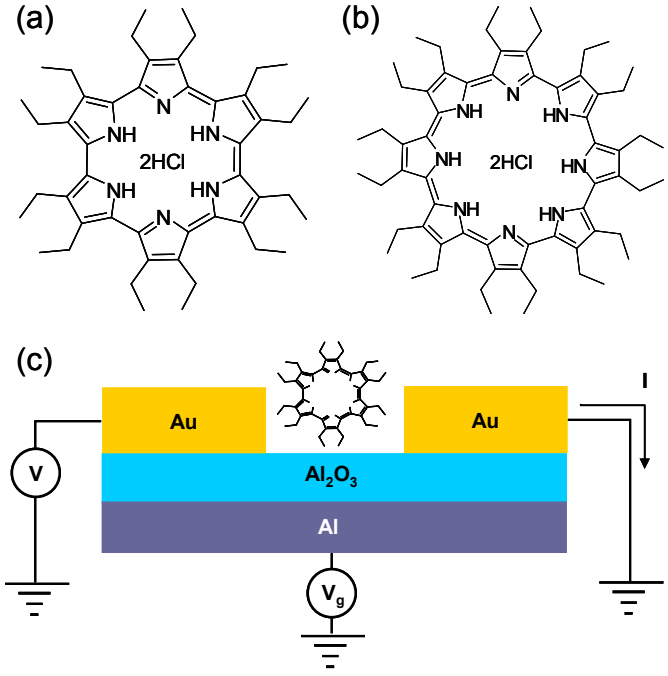

Figure 6.1 Single expanded-porphyrin transistor. (a) Structure of cyclo[6]pyrrole. (b) Structure of cyclo[8]pyrrole. (c) Schematic diagram of a device.

6.2 SAMPLE PREPARATION

A schematic representation of our single-molecule transistors is shown in Fig. 6.1(c). A dilute (~0.2 μM) solution of cyclo[*n*]pyrrole in dicholomethane is spin-deposited on Au nanowires with < 100 nm constrictions, which are fabricated by electron beam lithography. The electromigration is performed subsequently at low temperature in order to trap molecules in nanometer-sized gaps in-situ as described in Chapter 3. 28 out of 260 cyclo[6]pyrrole- and 13 out of 94 cyclo[8]pyrrole-devices show the Coulomb blockade behavior with strong gate modulation. For these devices, we measure

conductance in detail as a function of bias and gate voltages by numerically differentiating dc current-voltage curves or by ac lock-in technique at different gate voltages.

6.3 EXPERIMENTAL RESULTS

Figure 6.2 (a) shows a color plot of differential conductance on a logarithmic scale as a function of bias and gate voltages for a device incorporating cyclo[6]pyrrole (Device A). Dark and red colors correspond to low and high conductance values, respectively. Through capacitance coupling between the gate and the molecule, electrons are added (subtracted) one by one to (from) the molecule. There exists a degeneracy point between two distinct charge states as in a typical SET. The number of electrons in the inserted molecule increases (decreases) one by one whenever the gate voltage passes the degeneracy point in the positive (negative) direction. However, the initial charge state cannot be determined independently because it depends on the local electrostatic environment. Remarkably, zero-bias resonances (ZBRs) appear on both sides of the degeneracy point in two adjacent Coulomb blockaded regions. It implies that the suppression of conductance due to the Coulomb blockade effect is overcome at zero bias by a certain mechanism. In addition, the ZBRs have a strong gate dependence.

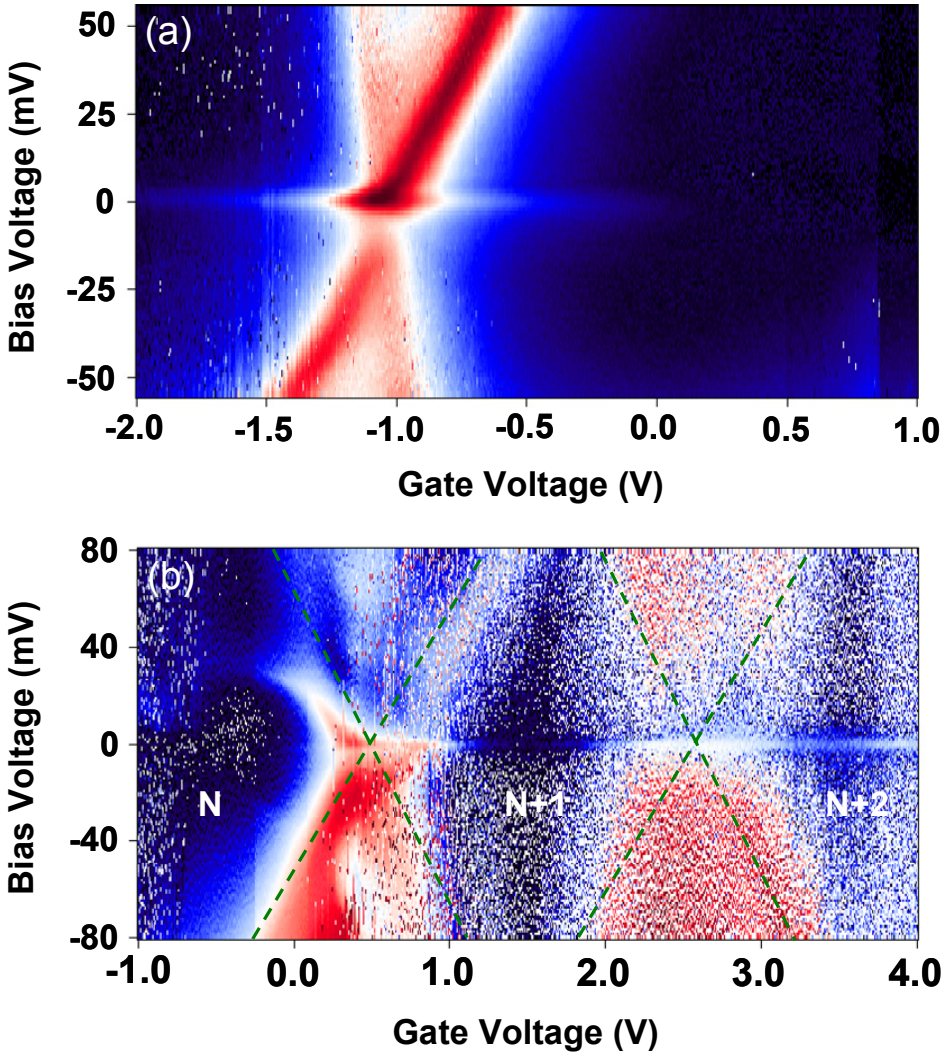

Figure 6.2 Differential conductance plots on logarithmic scale vs. bias and gate voltages in two single-cyclo[6]pyrrole transistors measured at 4.2 K. (a) Plot range from 10^{-9} to 10^{-7} S (Device A). (b) Plot range from 10^{-9} to 10^{-7} S (Device B). Green dashed lines are drawn to highlight the boundaries of the Coulomb blockaded regions.

Figure 6.2 (b) displays the conductance plot of another cyclo[6]pyrrole device (Device B). Three charged (redox) states are accessible within the gate range. If we assign N as the number of electrons in the molecule for the left Coulomb diamond, the central and right Coulomb diamonds correspond to the N+1 and N+2 charge states, respectively. The ZBRs are observed in the central and right Coulomb diamonds. The features are qualitatively similar to those of Device A. Thus, we can assign the observed redox states of Device A to the N+1 and N+2 charge states as in Device B. In the same Device B as shown in Fig. 6.2 (b), the ZBR disappears in the N charge state while the ZBR occurs in N+1 charge state like the conventional spin 1/2 Kondo effect with the parity behavior. Five more cyclo[6]pyrrole devices have exhibited ZBRs appearing in two adjacent Coulomb blockade regions as shown in Fig. 6.2 (a).

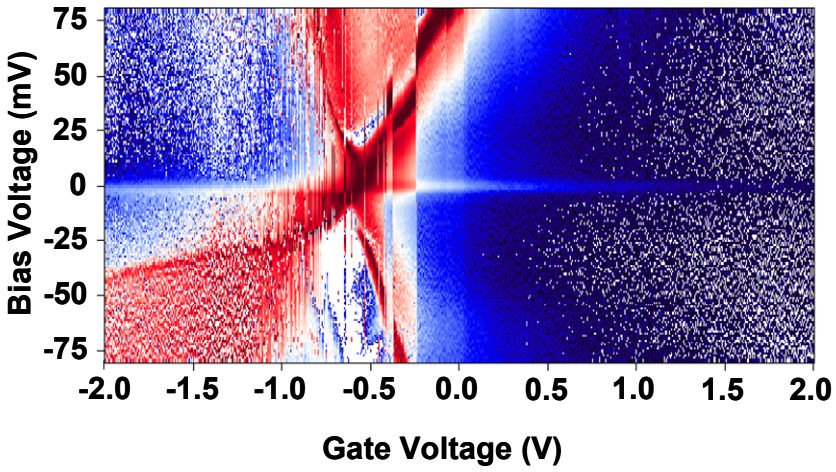

Figure 6.3 Conductance plot of a single-cyclo[8]pyrrole transistor as a function of bias and gate voltages measured at 4.2 K.

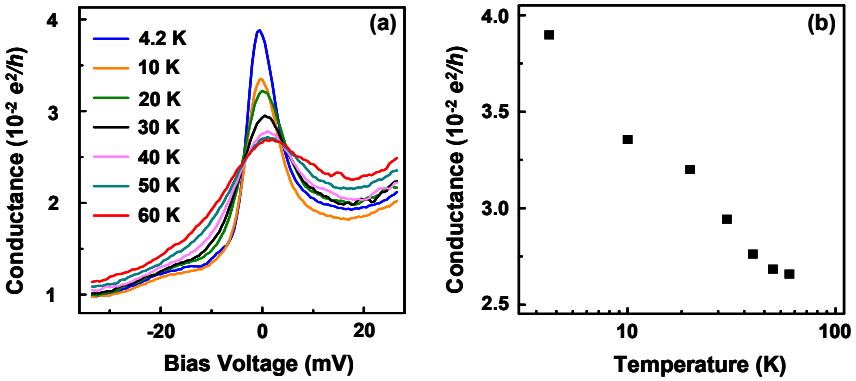

Figure 6.4 Temperature dependence of zero-bias resonance. (a) Plot of conductance at various temperatures. (b) Zero-bias conductance as a function of temperature.

We have measured the temperature dependence of the ZBR in a cyclo[6]pyrrole device similar to Device A (Fig. 6.4). With increasing temperature, the conductance value of the peak decreases as shown in Fig. 6.4 (a) as a signature of the Kondo resonance. A plot of the conductance peak height vs. temperature in Fig. 6.4 (b) shows that the height value approximately decreases in logarithmically with respect to temperature. The strong gate dependence of ZBR is also consistent with the Kondo resonance. As described in Chapter 2, the Kondo temperature representing the exchange strength is $T_K \approx (U\Gamma)^{1/2} e^{-\pi(\mu-\varepsilon_0)/2\Gamma}$, where U is the on-site electron repulsion energy, Γ is the width of the energy level, μ is the Fermi energy of the electrodes, and ε_0 is the energy level. For instance, if we increase the "distance" between the energy level and the Fermi energy using the gate voltage from degeneracy point toward a Coulomb blockade region, the Kondo temperature decreases. The Kondo temperature, T_K is also approximately estimated by the full width at half maximum of the Kondo resonance[19], FWHM~

$2k_{\mathrm{B}}T_{\mathrm{K}}/e$. Therefore, the width of the Kondo resonance becomes smaller and smaller as the gate voltage is tuned away from the degeneracy point. Figure 6.2 shows that the resonance features fade out from the degeneracy point. The two above characteristics strongly suggest that the observed ZBRs can be attributed to the Kondo effect.

6.4 DISCUSSIONS

In the simple spin ½ Kondo effect, a local spin in an isolated dot can be flipped by higher-order tunneling processes and the exchange interaction between the local spin and the conduction-electron spins in electrodes. Such a highly-correlated state gives rise to a ZBR known as the Kondo resonance. According to the constant interaction model[20] where the on-site Coulomb interaction is assumed a constant, which is described by a charging energy of the system, energy levels are filled with spin-up and spin-down electrons consecutively. When the number of electrons in the system is odd, the net spin becomes spin ½ and this leads to the Kondo resonance in a conductance measurement. When the number, on the other hand, is even, the spin-up and spin-down are paired up to the "top" energy level. It results in the zero net spin with no resonance. Since the electron numbers in SETs are controllable one by one, this odd-even parity behavior is observed. Obviously, this is not the case for the displayed data sets. Our observations and the above simple argument suggest that the constant interaction model cannot be a good approximation any more in this case.

We suggest a simple model that could describe the absence of the odd-even parity effect in the Kondo resonance. When an energy level is occupied by an electron as shown in Fig. 6.5 (a), the condition for the Kondo resonance is satisfied because the net spin is ½. For the next reduced state, it costs at least the charging energy to add one more electron to the molecule. In addition, several energy scales determine how the states are

filled with the extra electrons[21]: The exchange energy J that lowers the energy of the parallel spin configuration compared to the antiparallel one, the energy level spacing Δ between molecular orbitals, and the extra Coulomb energy δU to put two electrons in a single quantum state. There are two possible processes: When $J + \delta U > \Delta$, the second electron occupies the next level in the spin triplet state (Fig. 6.5 (a)→(b)). In contrast, the second electron occupies the lower energy level with opposite spins when $J + \delta U < \Delta$ (Fig. 6.5 (a)→(c)).

The proposed model provides us a natural explanation for all presented data sets. Based on the first scenario (Fig. 6.5 (a)→(b)), the ZBRs of the cyclo[6]pyrrole device in Fig.6. 2 (a) and those of a cyclo[8]pyrrole device in Fig. 6.3 are well described. If an unpaired spin is available in charge state on the left hand side, the Kondo resonance can occur like a conventional spin ½ Kondo effect. The next charge state on the right hand side can have the spin triplet configuration with even number electrons due to the strong exchange interaction. Thus, the net spin could be 1 and this can give rise to the Kondo resonance. The disappearance of the ZBR in Device B at N charge state as shown in Fig. 6.2 (b) can also be interpreted if the cyclo[6]pyrrole is in the zero spin state in the charge neutral state, which is consistent with a theoretical prediction[18] on this complex. In this device, the ground spin state follows the sequence of $S = 0 \rightarrow \frac{1}{2} \rightarrow 1$.

Interestingly, our observations of the absence of odd-even parity behavior are very similar to earlier reports for semiconducting quantum dots[22, 23] and carbon nanotubes[6, 7]. Those results show that when the exchange interaction is dominant in the systems with closely spaced energy levels, the Kondo resonances even occur for even number of electrons. Recently, L.H. Yu and his collaborators[14] have pointed out that the strong exchange interaction within the molecule could play a crucial role for the

interpretation of the similar experimental results in metal-based molecular devices. Our model can be understood based on the similar idea.

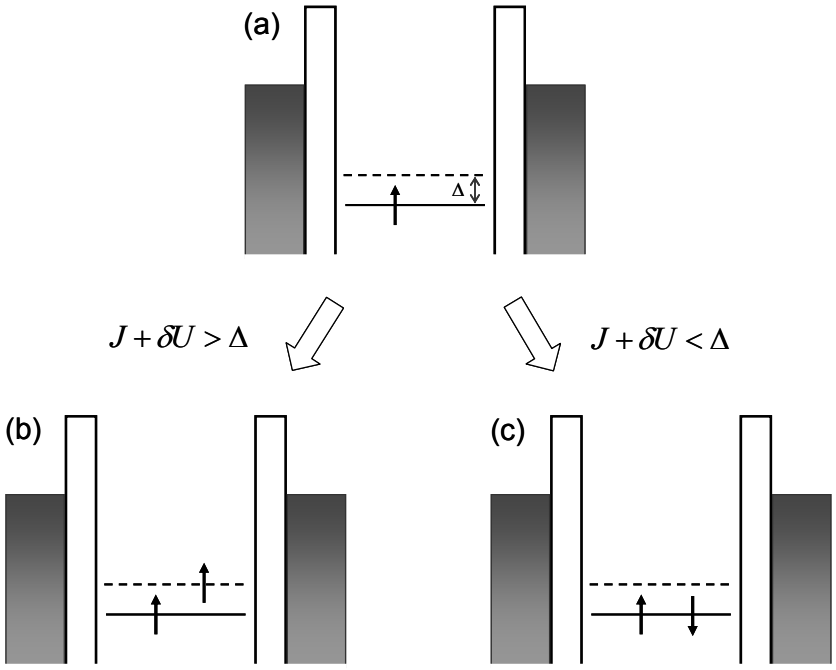

Figure 6.5 Schematic diagram of spin-filling with two excess electrons.

6.5 SUMMARY

In summary, we have observed a non-conventional Kondo effect in expanded porphyrin SMTs where the Kondo resonances at zero bias appear for both odd and even number of electrons. We have proposed a model in which the strong exchange interaction within the molecule leads to spin filling similar to Hund's rule, that is, the spin triplet is energetically more favorable to the spin singlet. We believe that more experimental and

theoretical studies are required to investigate the microscopic mechanisms. The exchange energy within the molecule is also needed to be estimated theoretically to understand the observation more quantitatively. Moveover, it would be interesting to test the theoretical prediction of the non-monotonic temperature dependence[24] of conductance in the Kondo resonance for S>1/2 in our system.

REFERENCES

[1] L. P. Kouwenhoven, C. M. Marcus, P. L. McEuen, S. Tarucha, R. M. Westervelt, and N. S. Wintergreen, in *Mesoscopic Electron Transport*, edited by L. P. Kouwenhoven, G. Schon and L. L. Shon (Kluwer Academic Publishers, Dordrecht, 1996).

[2] L. P. Kouwenhoven and L. I. Glazman, Physics World **14**, 33 (2001).

[3] D. Goldhaber-Gordon, H. Shtrikman, D. Mahalu, D. Abusch-Magder, U. Meirav, and M. A. Kastner, Nature **391**, 156 (1998).

[4] S. M. Cronenwett, T. H. Oosterkamp, and L. P. Kouwenhoven, Science **281**, 540 (1998).

[5] J. Nygard, D. H. Cobden, and P. E. Lindelof, Nature **408**, 342 (2000).

[6] W. J. Liang, M. Bockrath, and H. Park, Phys. Rev. Lett. **88**, 126801 (2002).

[7] B. Babic, T. Kontos, and C. Schonenberger, Phys. Rev. B **70**, 235419 (2004).

[8] P. Jarillo-Herrero, J. Kong, H. S. J. van der Zant, C. Dekker, L. P. Kouwenhoven, and S. De Franceschi, Nature **434**, 484 (2005).

[9] J. Paaske, A. Rosch, P. Wölfle, N. Mason, C. M. Marcus, and J. Nygård, Nature Phys. **2**, 460 (2006).

[10] W. J. Liang, M. P. Shores, M. Bockrath, J. R. Long, and H. Park, Nature **417**, 725 (2002).

[11] J. Park, A. N. Pasupathy, J. I. Goldsmith, C. Chang, Y. Yaish, J. R. Petta, M. Rinkoski, J. P. Sethna, H. D. Abruna, P. L. McEuen, and D. C. Ralph, Nature **417**, 722 (2002).

[12] L. H. Yu and D. Natelson, Nano Lett. **4**, 79 (2004).

[13] L. H. Yu, Z. K. Keane, J. W. Ciszek, L. Cheng, M. P. Stewart, J. M. Tour, and D. Natelson, Phys. Rev. Lett. **93**, 266802 (2004).

[14] L. H. Yu, Z. K. Keane, J. W. Ciszek, L. Cheng, J. M. Tour, T. Baruah, M. R. Pederson, and D. Natelson, Phys. Rev. Lett. **95**, 256803 (2005).

[15] A. N. Pasupathy, R. C. Bialczak, J. Martinek, J. E. Grose, L. A. K. Donev, P. L. McEuen, and D. C. Ralph, Science **306**, 86 (2004).

[16] T. Kohler, D. Seidel, V. Lynch, F. O. Arp, Z. P. Ou, K. M. Kadish, and J. L. Sessler, J. Am. Chem. Soc. **125**, 6872 (2003).

[17] D. Seidel, V. Lynch, and J. L. Sessler, Angew. Chem., Int. Ed. **41**, 1422 (2002).

[18] A. Gorski, T. Kohler, D. Seidel, J. T. Lee, G. Orzanowska, J. L. Sessler, and J. Waluk, Chem.-Eur. J. **11**, 4179 (2005).

[19] W. G. van der Wiel, S. De Franceschi, T. Fujisawa, J. M. Elzerman, S. Tarucha, and L. P. Kouwenhoven, Science **289**, 2105 (2000).

[20] L. P. Kouwenhoven, D. G. Austing, and S. Tarucha, Rep. Prog. Phys. **64**, 701 (2001).

[21] Y. Oreg, K. Byczuk, and B. I. Halperin, Phys. Rev. Lett. **85**, 365 (2000).

[22] J. Schmid, J. Weis, K. Eberl, and K. von Klitzing, Phys. Rev. Lett. **84**, 5824 (2000).

[23] A. Kogan, G. Granger, M. A. Kastner, D. Goldhaber-Gordon, and H. Shtrikman, Phys. Rev. B **67**, 113309 (2003).

[24] M. Pustilnik and L. I. Glazman, Phys. Rev. Lett. **8721**, 216601 (2001).

Chapter 7. Ongoing Projects: Progress and Future Outlook

7.1 INTRODUCTION

Spin-dependent transport behavior has been investigated for several decades to understand the fundamental physics as well as to realize the spin-based electronics[1]. The Coulomb blockade effect[2] in transport through nanostuctures, on the other hand, has been actively studied and has been well-established. It is expected that the combination of these two attractive research areas can give rise to a qualitatively new research regime that is not accessible for either non-interacting or spin-independent electron transport. Recently, researchers started investigating this exciting regime intensively from both theoretical[3-5] and experimental[6-8] points of view. Our interests have been motivated under this vision. In this chapter, we describe our projects including the Kondo effect in the presence of ferromagnetic electrodes and the spin-dependent electron transport in single-wall carbon nanotube through highly transparent contacts.

7.2 KONDO EFFECT IN SINGLE MOLECULES COUPLED TO FERROMAGNETIC ELECTRODES

Several mechanisms are expected to influence the Kondo effect in the presence of ferromagnetism as follows[3]. First, the finite spin-polarization of electrodes can influence the Kondo behavior. Spin-up and spin-down electrons are essential to screen the local spin effectively. An imbalance of spins in the ferromagnetic electrodes weakens the spin screening capability. It is expected to result in the decrease of the Kondo temperature. Second, the strong exchange interaction between the molecule and the ferromagnetic electrodes leads to an exchange field analogous to an external magnetic field. Thus, the spin degeneracy can be lifted like the Zeeman splitting. A recent experiment[7] has

confirmed that the Kondo resonance is indeed split and suppressed in the presence of ferromagnetic electrodes. This work[7] leaves several questions open at the same time. For instance, the mechanisms responsible for the observed negative value and enhancement of the magnetoresistance (MR) are poorly understood. In addition, no gate modulation of the inserted molecules is shown. Our project was initiated in order to answer these questions and to understand the interplay of the Kondo effect and ferromagnetism more systematically.

We have adopted the electromigration break junction technique to realize a nanometer-sized gap between ferromagnetic electrodes. Two different diamond-shaped permalloy electrodes are connected to each other through a 100 nm narrow constriction with a thickness of 10 nm (Fig. 7.1 (a)). The long axes of the electrodes are oriented horizontally in order to make an easy magnetic axis along the axis. In addition, different geometric aspect ratios are used to obtain two different coercive fields to realize the parallel and antiparallel configurations of magnetizations. So far, we have demonstrated that the structure could be broken to create a small gap in the absence of molecule and the tunneling MR has been observed depending on the relative orientation of magnetizations. The resistance is maximal for antiparallel alignment whereas it is minimal for parallel alignment as shown in Fig. 7.1 (b). Currently, we are optimizing the experimental procedure to trap Co-porphyrins.

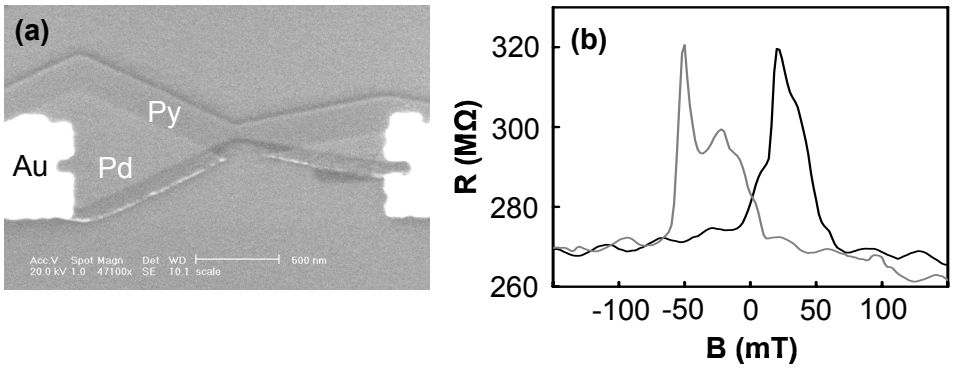

Figure 7.1 Tunneling magnetoresistance. (a) Scanning electron micrograph of ferromagnetic nanoconstriction. (b) Resistance vs. external magnetic field.

7.3 SPIN-DEPENDENT TRANSPORT IN SINGLE-WALL CARBON NANOTUBES

Another interesting project is an experimental study of spin-dependent transport in single-wall carbon nanotube, which possesses several intriguing properties[9] for the spin-dependent transport. Single-wall carbon nanotube (SWNT) is considered as an ideal system for spin-dependent transport studies since the spin coherent length is expected to be long due to the ballistic characteristics and negligible spin-orbit coupling. In addition, it is relatively easy to make SWNT devices compared to single molecule devices because the fabrication is more controllable.

We have fabricated SWNT devices as follows. SWNT is connected to permalloy electrodes and capacitively coupled to a back-gate. Atomic force micrograph of a device is shown in the inset in Fig. 7.3. Two different geometric aspect ratios of rectangular ferromagnetic electrodes are used to obtain two different coercive fields to realize the parallel and antiparallel configurations of magnetizations. The length of the SWNT is about 250 nm between the electrodes. The SWNT is contacted on the 13 nm permalloy

electrodes and the 15 nm Pd capping layer is shifted using shadow evaporation so as not to touch the SWNT. We have investigated the spin-dependent transport at 4.2 K by controlling the relative magnetizations with an external magnetic field along the long axes of electrodes.

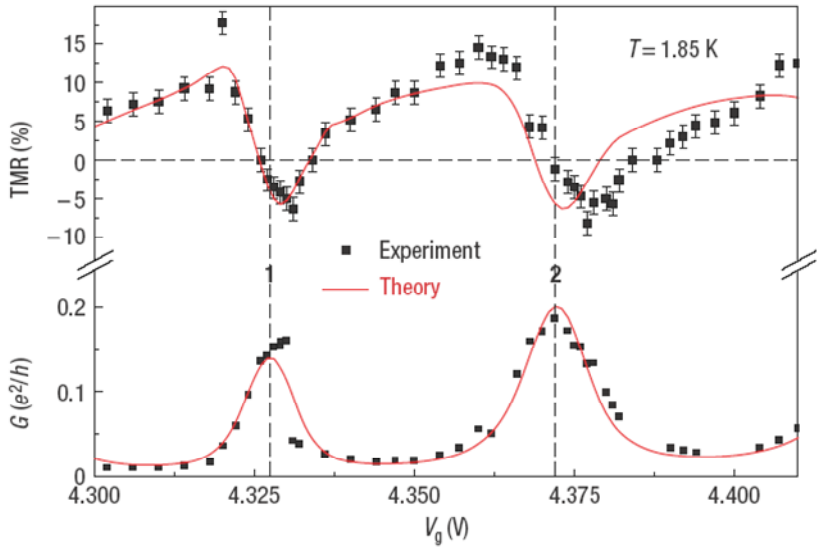

Figure 7.2 Gate modulated magnetoresistance (from Ref. 6).

Recently, Sahoo and her collaborators[6] have reported that the sign and the magnitude of MR are oscillatory in SWNT-devices in the Coulomb blockade regime as shown in Fig. 7.2. The lower panel shows conductance as a function of gate voltage and the upper panel shows the exotic oscillatory behavior of MR. According to the spin-dependent resonance tunneling model[4, 6, 10], the spin-dependent tunneling at resonance can invert the ordinary positive MR into the negative value and the modulation of the magnitude can be tuned with a gate voltage depending on how a quantum state in SWNT is aligned with respect to the Fermi energy of ferromagnetic electrodes. We have also reproduced the results.

Remarkably, we have also investigated spin transport in a device exhibiting an interference pattern and Kondo resonance as shown in Fig. 7.3 (a). Figure 7.3 (b) shows that the conductance at zero bias is close to the ideal value ($4e^2/h$) for SWNT. This implies that this device is connected to the ferromagnetic electrodes with highly transparent contacts. The interference pattern resembles the Fabry-Pérot interference as reported in non-magnetic SWNT devices[11]. Differential conductance is oscillatory along both bias and gate voltages. Since the Fermi-energy in SWNT can be tuned by the bias and gate voltages, the Fermi wave number for electrons in SWNT changes. This modulation gives rise to the oscillation of the differential conductance analogous to the Fabry-Pérot interference in an optical system. That is, electron waves are multiply reflected between two SWNT-ferromagnetic metal interfaces like an optical cavity in an interference etalon. Interestingly, the conductance plot also shows that the zero-bias resonances are clearly shown with the parity effect between about 1 V and 6 V of gate voltage in the same device. The logarithmic temperature dependence of the resonance at gate voltage of 1.8 V confirms that the resonance is attributed to the Kondo effect.

We have carried out the MR measurements in both regimes. For instance, gate voltage of -4.5 V (marked by a blue arrow) and 1.8 V (marked by a red arrow) are selected for the interference and the Kondo regimes, respectively. The conductance is measured as a function of bias voltage with a gate voltage fixed by sweeping an external magnetic field to achieve parallel and antiparallel configurations of magnetizations. The external magnetic field is first ramped up to 200 mT to align the magnetizations in electrodes in parallel. The field is then reduced down to -200 mT during which the conductance is being measured. The relative magnetizations become antiparallel between -5 mT and -20 mT in the device as shown in Fig. 7.4 (a) and (b). There are profound changes in conductance. Figure 7.4 (c) and (d) show MRs for the interference and the

Kondo regimes, respectively. After selecting conductance curves for the parallel and antiparallel configurations, the conductance values of antiparallel case is subtracted from those of the parallel case at each bias voltage and the values are normalized by the conductance values for the antiparallel case. In both regimes, MRs are oscillatory in the sign and the magnitute (2~5 %) up to at least ±15 mV in bias voltage. More interestingly, we have observed only positive MR (1~ 3%) at zero bias in the Kondo valley region around gate voltage of 1.8 V between two adjacent degeneracy points (not shown here). This behavior is inconsistent with previous theoretical[3] and experimental[7] predicting results that the Kondo peak is split in the parallel case in the presence of ferromagnetism owing to the exchange field while the resonance is not suppressed in the antiparallel case, leading to negative MR values.

Our device in Fig. 7.3 is in a more transparent regime than the device in Fig. 7.2, which is in the interacting Coulomb blockade regime. Nevertheless, it is expected that when the Kondo effect is observed, the quantum dot can be "effectively" regarded as non-interacting system[12]. In addition, if we assume that electron-electron interaction is negligible in the interference regime, all the regimes can be understood with a non-interacting resonance model with some effective parameters[12]. Currently, the interpretation on the observations of the oscillatory MRs and the zero bias positive MRs in the Kondo valley region is under way in the spirit of the spin-dependence of interfacial phase shift in the transport.

Another interesting future project with SWNT devices is an experimental observation of the spin-charge separation in one-dimensional system, that is, the spin and charge degrees of freedom are believed to be completely decoupled and propagate with different velocities. Balents and Egger have theoretically proposed how to observe this

exotic phenomenon using SWNT as a one-dimensional quantum wire[13, 14]. We will carry out experiments based on their proposal in the future.

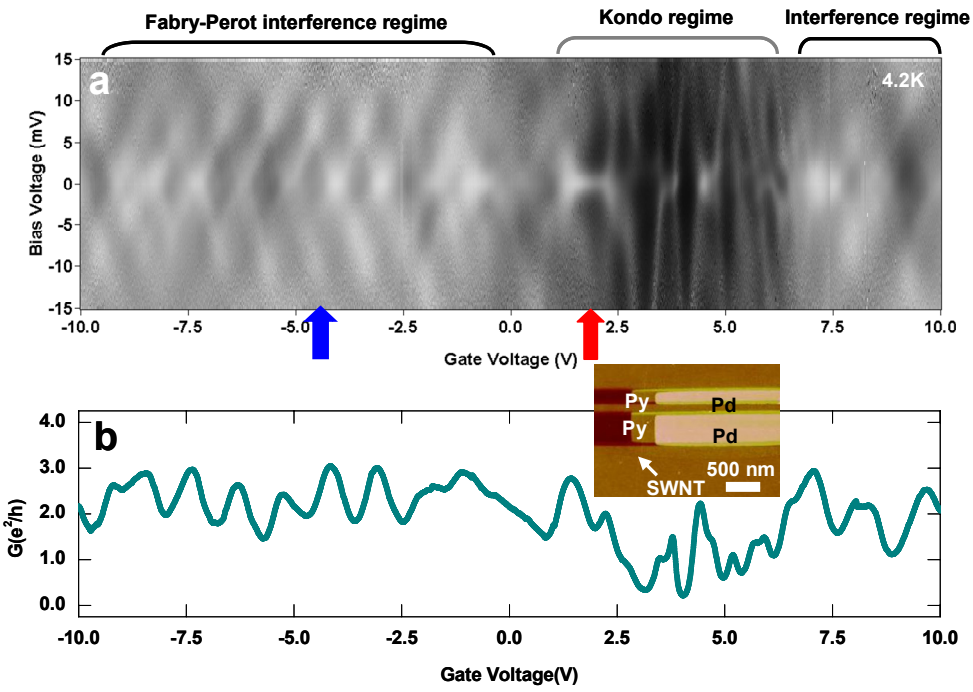

Figure 7.3 Conductance measurement of a SWNT transistor (Courtesy of S. Jung). (a) Plot of differential conductance as a function of gate and bias voltages. (b) Conductance at zero bias with respect to gate voltage. The inset shows atomic force micrograph of the device.

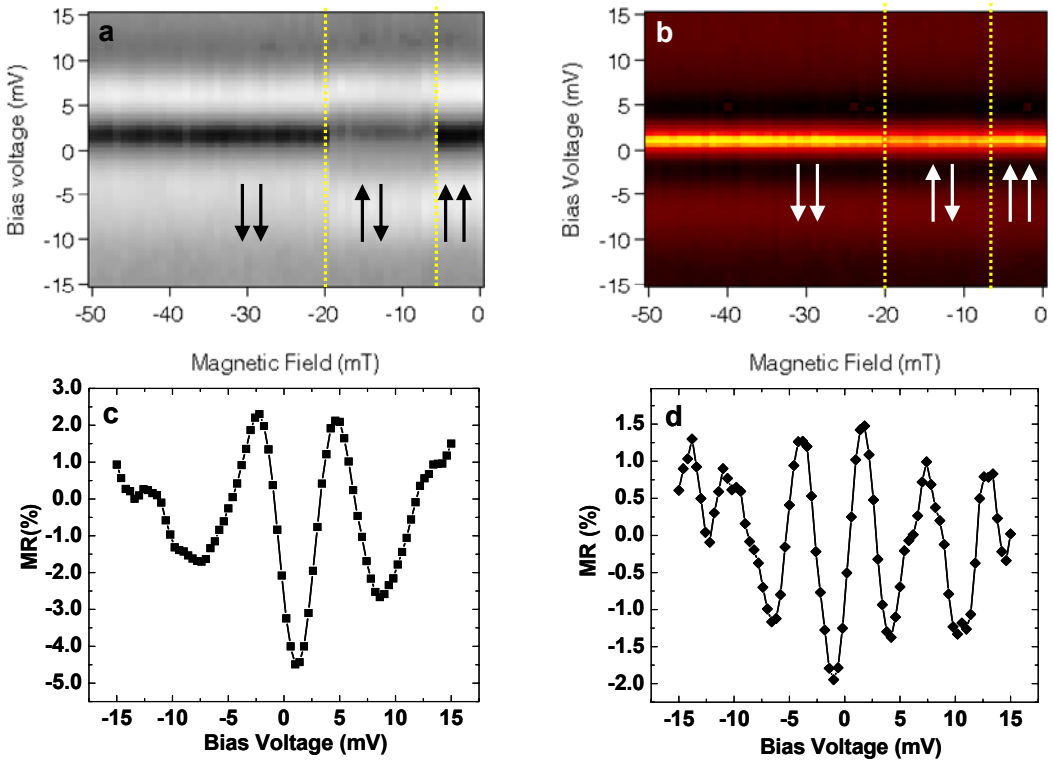

Figure 7.4 Magnetoresistance measurements (Courtesy of S. Jung). (a) Conductance plot as a function of bias and external magnetic field at -4.5 V of gate voltage. (b) Conductance plot as a function of bias voltage and external magnetic field at 1.8 V of gate voltage. (c) MR vs. bias voltage at a gate voltage of -4.5V in the Fabry-Pérot interference regime. (d) MR vs. bias voltage at a gate voltage of 1.8V in the Kondo regime.

7.4 SUMMARY

In this chapter, we have described our on-going endeavors to understand the interplay of the spin degree of freedom and ferromagnetism. First, we have tried to realize a molecule coupled to ferromagnetic leads in order to understand how the Kondo effect is affected by the exchange field. Second, we have investigated SWNT-transistors

using ferromagnetic electrodes to study how the MR is influenced by the bias and gate voltages in the interference and the Kondo regimes.

REFERENCES

[1] S. A. Wolf, D. D. Awschalom, R. A. Buhrman, J. M. Daughton, S. von Molnar, M. L. Roukes, A. Y. Chtchelkanova, and D. M. Treger, Science **294**, 1488 (2001).

[2] L. P. Kouwenhoven, C. M. Marcus, P. L. McEuen, S. Tarucha, R. M. Westervelt, and N. S. Wintergreen, in *Mesoscopic Electron Transport*, edited by L. P. Kouwenhoven, G. Schon and L. L. Shon (Kluwer Academic Publishers, Dordrecht, 1996).

[3] J. König, J. Martinek, J. Barna, and G. Schön, in *CFN Lectures on Functional Nanostructures*, edited by K. Busch, A. Powell, C. Röthig, G. Schön and J. Weissmüller (Springer, Berlin / Heidelberg, 2005), Vol. 1.

[4] A. Cottet, T. Kontos, W. Belzig, C. Schonenberger, and C. Bruder, Europhys. Lett. **74**, 320 (2006).

[5] A. Cottet and M. Choi, cond-mat/0605264.

[6] S. Sahoo, T. Kontos, J. Furer, C. Hoffmann, M. Gräber, A. Cottet, and C. Schönenberger, Nature Phys. **2**, 320 (2006).

[7] A. N. Pasupathy, R. C. Bialczak, J. Martinek, J. E. Grose, L. A. K. Donev, P. L. McEuen, and D. C. Ralph, Science **306**, 86 (2004).

[8] H. T. Man, I. J. W. Wever, and A. F. Morpurgo, cond-mat/0512505 (2005).

[9] C. Dekker, Physics Today **52**, 22 (1999).

[10] E. Y. Tsymbal, A. Sokolov, I. F. Sabirianov, and B. Doudin, Phys. Rev. Lett. **90** (2003).

[11] W. J. Liang, M. Bockrath, D. Bozovic, J. H. Hafner, M. Tinkham, and H. Park, Nature **411**, 665 (2001).

[12] M. Choi, private communication.

[13] L. Balents and R. Egger, Phys. Rev. Lett. **85**, 3464 (2000).

[14] L. Balents and R. Egger, Phys. Rev. B **64**, 035310 (2001).

Bibliography

Note: Each chapter has a reference section. In this bibliography, reference materials, which are used in this dissertation, are sorted in alphabetical order of the first author.

M. Abe, T. Kitagawa, and Y. Kyogoku, J. Chem. Phys. **69**, 4526 (1978).

D. V. Averin and Y. V. Nazarov, in *Single Charge Tunneling: Coulomb Blockade Phenomena in Nanostructures*, edited by H. Grabert and M. H. Devoret (Plenum Press and NATO Science Affairs Division, New York, 1992).

A. Aviram and M. A. Ratner, Chem. Phys. Lett. **29**, 277 (1974).

B. Babic, T. Kontos, and C. Schonenberger, Phys. Rev. B **70**, 235419 (2004).

L. Balents and R. Egger, Phys. Rev. Lett. **85**, 3464 (2000).

L. Balents and R. Egger, Phys. Rev. B **64**, 035310 (2001).

J. K. Bera and K. R. Dunbar, Angew. Chem., Int. Ed. **41**, 4453 (2002).

J. F. Berry, in *Multiple Bonds between Metal Atoms*, edited by F. A. Cotton, C. A. Murillo and R. A. Walton (Springer, New York, 2005).

J. F. Berry, F. A. Cotton, L. M. Daniels, and C. A. Murillo, J. Am. Chem. Soc. **124**, 3212 (2002).

J. F. Berry, F. A. Cotton, L. M. Daniels, C. A. Murillo, and X. P. Wang, Inorg. Chem. **42**, 2418 (2003).

J. F. Berry, F. A. Cotton, P. Lei, T. Lu, and C. A. Murillo, Inorg. Chem. **42**, 3534 (2003).

J. F. Berry, F. A. Cotton, P. Lei, and C. A. Murillo, Inorg. Chem. **42**, 377 (2003).

N. E. Bickers, Rev. Mod. Phys. **59**, 845 (1987).

M. J. Biercuk, S. Garaj, N. Mason, J. M. Chow, and C. M. Marcus, Nano Lett. **5**, 1267 (2005).

K. I. Bolotin, F. Kuemmeth, A. N. Pasupathy, and D. C. Ralph, Appl. Phys. Lett.

84, 3154 (2004).

D. Chae, J. F. Berry, S. Jung, F. A. Cotton, C. A. Murillo, and Z. Yao, Nano Lett. **6**, 165 (2006).

D. Chae, J. Lee, J. L. Sessler, and Z. Yao, In preparation (2006).

J. Chen, M. A. Reed, A. M. Rawlett, and J. M. Tour, Science **286**, 1550 (1999).

J. Chen, M. A. Reed, A. M. Rawlett, and J. M. Tour, Science **286**, 1550 (1999).

P. S. Cornaglia, H. Ness, and D. R. Grempel, Phys. Rev. Lett. **93**, 147201 (2004).

A. Cottet and M. Choi, cond-mat/0605264.

A. Cottet, T. Kontos, W. Belzig, C. Schonenberger, and C. Bruder, Europhys. Lett. **74**, 320 (2006).

F. A. Cotton and R. A. Walton, Multi Bonds Between Metal Atoms (Clarendon, Oxford, 2nd edn., 1993).

S. M. Cronenwett, T. H. Oosterkamp, and L. P. Kouwenhoven, Science **281**, 540 (1998).

X. D. Cui, A. Primak, X. Zarate, J. Tomfohr, O. F. Sankey, A. L. Moore, T. A. Moore, D. Gust, G. Harris, and S. M. Lindsay, Science **294**, 571 (2001).

S. De Franceschi, S. Sasaki, J. M. Elzerman, W. G. van der Wiel, S. Tarucha, and L. P. Kouwenhoven, Phys. Rev. Lett. **86**, 878 (2001).

C. Dekker, Physics Today **52**, 22 (1999).

D. Dolphin, *The Porphyrins* (Academic, New York, 1978).

D. Dulic, S. J. van der Molen, T. Kudernac, H. T. Jonkman, J. J. D. de Jong, T. N. Bowden, J. van Esch, B. L. Feringa, and B. J. van Wees, Phys. Rev. Lett. **91** (2003).

T. M. Eiles, J. M. Martinis, and M. H. Devoret, Phys. Rev. Lett. **70**, 1862 (1993).

J. Fuhrhop, K. Kadiah, and G. Davis, J. Am. Chem. Soc. **95**, 5140 (1973).

T. A. Fulton and G. J. Dolan, Phys. Rev. Lett. **59**, 109 (1987).

I. Giaever and H. R. Zeller, Phys. Rev. Lett. **20**, 1504 (1968).

L. I. Glazman and R. I. Shekhter, J. Phys. Condens. Matter **1**, 5811 (1989).

D. Goldhaber-Gordon, J. Gores, M. A. Kastner, H. Shtrikman, D. Mahalu, and U. Meirav, Phys. Rev. Lett. **81**, 5225 (1998).

D. Goldhaber-Gordon, H. Shtrikman, D. Mahalu, D. Abusch-Magder, U. Meirav, and M. A. Kastner, Nature **391**, 156 (1998).

A. Gorski, T. Kohler, D. Seidel, J. T. Lee, G. Orzanowska, J. L. Sessler, and J. Waluk, Chem.-Eur. J. **11**, 4179 (2005).

L. Gruter, F. Y. Cheng, T. T. Heikkila, M. T. Gonzalez, F. O. Diederich, C. Schonenberger, and M. Calame, Nanotechnology **16**, 2143 (2005).

H. B. Heersche, Z. de Groot, J. A. Folk, L. P. Kouwenhoven, H. S. J. van der Zant, A. A. Houck, J. Labaziewicz, and I. L. Chuang, Phys. Rev. Lett. **96**, 206801 (2006).

A. A. Houck, J. Labaziewicz, E. K. Chan, J. A. Folk, and I. L. Chuang, Nano Lett. **5**, 1685 (2005).

P. Jarillo-Herrero, J. Kong, H. S. J. van der Zant, C. Dekker, L. P. Kouwenhoven, and S. De Franceschi, Nature **434**, 484 (2005).

P. Jarillo-Herrero, S. Sapmaz, C. Dekker, L. P. Kouwenhoven, and H. S. J. van der Zant, Nature **429**, 389 (2004).

C. Joachim, J. K. Gimzewski, R. R. Schlittler, and C. Chavy, Phys. Rev. Lett. **74**, 2102 (1995).

C. Kergueris, J. P. Bourgoin, S. Palacin, D. Esteve, C. Urbina, M. Magoga, and C. Joachim, Physical Review B **59**, 12505 (1999).

P. Kiehl, M. M. Rohmer, and M. Benard, Inorganic Chemistry **43**, 3151 (2004).

J. Koch and F. von Oppen, Phys. Rev. Lett. **94**, 206804 (2005).

J. Koch, F. von Oppen, and A. V. Andreev, cond-mat/0606512 (2006).

A. Kogan, G. Granger, M. A. Kastner, D. Goldhaber-Gordon, and H. Shtrikman, Phys. Rev. B **67**, 113309 (2003).

T. Kohler, D. Seidel, V. Lynch, F. O. Arp, Z. P. Ou, K. M. Kadish, and J. L. Sessler, J. Am. Chem. Soc. **125**, 6872 (2003).

J. König, J. Martinek, J. Barna, and G. Schön, in *CFN Lectures on Functional Nanostructures*, edited by K. Busch, A. Powell, C. Röthig, G. Schön and J. Weissmüller (Springer, Berlin / Heidelberg, 2005), Vol. 1.

L. P. Kouwenhoven, D. G. Austing, and S. Tarucha, Rep. Prog. Phys. **64**, 701 (2001).

L. P. Kouwenhoven and L. I. Glazman, Physics World **14**, 33 (2001).

L. P. Kouwenhoven, C. M. Marcus, P. L. McEuen, S. Tarucha, R. M. Westervelt, and N. S. Wintergreen, in *Mesoscopic Electron Transport*, edited by L. P. Kouwenhoven, G. Schon and L. L. Shon (Kluwer Academic Publishers, Dordrecht, 1996).

L. P. Kouwenhoven, T. H. Oosterkamp, M. W. S. Danoesastro, M. Eto, D. G. Austing, T. Honda, and S. Tarucha, Science **278**, 1788 (1997).

S. Kubatkin, A. Danilov, M. Hjort, J. Cornil, J. L. Bredas, N. Stuhr-Hansen, P. Hedegard, and T. Bjornholm, Nature **425**, 698 (2003).

J. Lambe and R. C. Jaklevic, Phys. Rev. Lett. **22**, 1371 (1969).

L. D. Landau and E. M. Lifshitz, *Mechanics* (Pergamon Press, New York, 1976).

X. Y. Li, R. S. Czernuszewicz, J. R. Kincaid, Y. O. Su, and T. G. Spiro, J. Phys. Chem. **94**, 31 (1990).

W. J. Liang, M. Bockrath, D. Bozovic, J. H. Hafner, M. Tinkham, and H. Park, Nature **411**, 665 (2001).

W. J. Liang, M. Bockrath, and H. Park, Phys. Rev. Lett. **88**, 126801 (2002).

W. J. Liang, M. P. Shores, M. Bockrath, J. R. Long, and H. Park, Nature **417**, 725 (2002).

W. J. Liang, M. P. Shores, M. Bockrath, J. R. Long, and H. Park, Nature **417**, 725 (2002).

G. Lientschnig, PhD thesis, Delft University of Technology (2003).

K. K. Likharev, Proc. IEEE **87**, 606 (1999).

V. Madhavan, W. Chen, T. Jamneala, M. F. Crommie, and N. S. Wingreen, Science **280**, 567 (1998).

H. T. Man, I. J. W. Wever, and A. F. Morpurgo, cond-mat/0512505 (2005).

P. L. McEuen, E. B. Foxman, U. Meirav, M. A. Kastner, Y. Meir, N. S. Wingreen, and S. J. Wind, Phys. Rev. Lett. **66**, 1926 (1991).

Y. Meir, N. S. Wingreen, and P. A. Lee, Phys. Rev. Lett. **26**, 2601 (1993).

T. K. Ng and P. A. Lee, Phys. Rev. Lett. **61**, 1768 (1988).

A. Nitzan and M. A. Ratner, Science **300**, 1384 (2003).

J. Nygard, D. H. Cobden, and P. E. Lindelof, Nature **408**, 342 (2000).

W. A. Oertling, A. Salehi, Y. C. Chung, G. E. Leroi, C. K. Chang, and G. T. Babcock, J. Phys. Chem. **91**, 5887 (1987).

T. H. Oosterkamp, J. W. Janssen, L. P. Kouwenhoven, D. G. Austing, T. Honda, and S. Tarucha, Phys. Rev. Lett. **82**, 2931 (1999).

Y. Oreg, K. Byczuk, and B. I. Halperin, Phys. Rev. Lett. **85**, 365 (2000).

H. Oshio, H. Spiering, V. Ksenofontov, F. Renz, and P. Gutlich, Inorg. Chem. **40**, 1143 (2001).

J. Paaske, A. Rosch, P. Wölfle, N. Mason, C. M. Marcus, and J. Nygård, Nature Phys. **2**, 460 (2006).

H. Park, A. K. L. Lim, A. P. Alivisatos, J. Park, and P. L. McEuen, Appl. Phys. Lett. **75**, 301 (1999).

H. Park, J. Park, A. K. L. Lim, E. H. Anderson, A. P. Alivisatos, and P. L. McEuen, Nature **407**, 57 (2000).

J. Park, A. N. Pasupathy, J. I. Goldsmith, C. Chang, Y. Yaish, J. R. Petta, M. Rinkoski, J. P. Sethna, H. D. Abruna, P. L. McEuen, and D. C. Ralph, Nature **417**, 722 (2002).

A. N. Pasupathy, R. C. Bialczak, J. Martinek, J. E. Grose, L. A. K. Donev, P. L. McEuen, and D. C. Ralph, Science **306**, 86 (2004).

A. N. Pasupathy, J. Park, C. Chang, A. V. Soldatov, S. Lebedkin, R. C. Bialczak, J. E. Grose, L. A. K. Donev, J. P. Sethna, D. C. Ralph, and P. L. McEuen, Nano Lett. **5**, 203 (2005).

J. R. Petta, D. G. Salinas, and D. C. Ralph, Appl. Phys. Lett. **77**, 4419 (2000).

D. Porath, Y. Levi, M. Tarabiah, and O. Millo, Phys. Rev. B **56**, 9829 (1997).

M. Pustilnik and L. I. Glazman, Phys. Rev. Lett. **8721**, 216601 (2001).

M. A. Reed, C. Zhou, C. J. Muller, T. P. Burgin, and J. M. Tour, Science **278**, 252 (1997).

S. Sahoo, T. Kontos, J. Furer, C. Hoffmann, M. Gräber, A. Cottet, and C. Schönenberger, Nature Phys. **2**, 320 (2005).

J. Schmid, J. Weis, K. Eberl, and K. von Klitzing, Phys. Rev. Lett. **84**, 5824 (2000).

J. H. F. Scottthomas, S. B. Field, M. A. Kastner, H. I. Smith, and D. A. Antoniadis, Phys. Rev. Lett. **62**, 583 (1989).

D. Seidel, V. Lynch, and J. L. Sessler, Angew. Chem., Int. Ed. **41**, 1422 (2002).

D. F. Shriver and C. B. Cooper, in *Advances in Infrared and Raman Spectroscopy*, edited by R. J. H. Clark and R. E. Hester (John Wiley, New York, 1979), Vol. 6.

R. H. M. Smit, Y. Noat, C. Untiedt, N. D. Lang, M. C. van Hemert, and J. M. van Ruitenbeek, Nature **419**, 906 (2002).

B. C. Stipe, M. A. Rezaei, and W. Ho, Science **280**, 1732 (1998).

S. Tarucha, D. G. Austing, T. Honda, R. J. vanderHage, and L. P. Kouwenhoven, Phys. Rev. Lett. **77**, 3613 (1996).

M. Tinkham, *Introduction to Superconductivity* (McGraw-Hill, New York, 1996).

W. G. van der Wiel, S. De Franceschi, T. Fujisawa, J. M. Elzerman, S. Tarucha, and L. P. Kouwenhoven, Science **289**, 2105 (2000).

D. A. van Leeuwen, J. M. van Ruitenbeek, L. J. Dejongh, A. Ceriotti, G. Pacchioni, O. D. Haberlen, and N. Rosch, Phys. Rev. Lett. **73**, 1432 (1994).

J. M. van Ruitenbeek, A. Alvarez, I. Pineyro, C. Grahmann, P. Joyez, M. H. Devoret, D. Esteve, and C. Urbina, Rev. Sci. Instr. **67**, 108 (1996).

P. Wahl, L. Diekhoner, G. Wittich, L. Vitali, M. A. Schneider, and K. Kern, Phys. Rev. Lett. **95,** 166601 (2005).

W. Y. Wang, T. Lee, I. Kretzschmar, and M. A. Reed, Nano Lett. **4**, 643 (2004).

E. M. Weig, R. H. Blick, T. Brandes, J. Kirschbaum, W. Wegscheider, M. Bichler, and J. P. Kotthaus, Phys. Rev. Lett. **92**, 046804 (2004).

J. Weis, in *CFN Lectures on Functional Nanostructures* edited by K. Busch, A. Powell, C. Röthig, G. Schön and J. Weissmüller (Springer Berlin/Heidelberg, 2005), Vol. 1.

S. A. Wolf, D. D. Awschalom, R. A. Buhrman, J. M. Daughton, S. von Molnar, M. L. Roukes, A. Y. Chtchelkanova, and D. M. Treger, Science **294**, 1488 (2001).

C. Y. Yeh, C. H. Chou, K. C. Pan, C. C. Wang, G. H. Lee, Y. O. Su, and S. M. Peng, J. Chem. Soc., Dalton Trans., 2670 (2002).

L. H. Yu, Z. K. Keane, J. W. Ciszek, L. Cheng, M. P. Stewart, J. M. Tour, and D. Natelson, Phys. Rev. Lett. **93**, 266802 (2004).

L. H. Yu, Z. K. Keane, J. W. Ciszek, L. Cheng, J. M. Tour, T. Baruah, M. R. Pederson, and D. Natelson, Phys. Rev. Lett. **95**, 256803 (2005).

L. H. Yu and D. Natelson, Nano Lett. **4**, 79 (2004).

A. D. Zhao, Q. X. Li, L. Chen, H. J. Xiang, W. H. Wang, S. Pan, B. Wang, X. D. Xiao, J. L. Yang, J. G. Hou, and Q. S. Zhu, Science **309**, 1542 (2005).

Vita

Dong-Hun Chae was born in Kong-Gum, Sangju, Kyungbuk, Republic of Korea on December 20, 1973, the son of HongBaek Chae and BongAe Kim. His childhood was filled with a variety of activities in the Mother Nature including fishing, swimming in creeks, gathering strawberry and chestnuts and snow-sledding in mountains. After completing B.A. in Physics Department at Chungnam National University, Daejon, Korea, in 1996, he started his master project in Physics Department at Pohang University of Science and Technology, Korea in the same year. He carried out experiments with magnetic multilayer structures using the synchrotron radiation of the Pohang Light Source in the Institute under supervising of Prof. Ki-Bong Lee until he finished his master degree in 1998. After mandatory civil service for one and half a year in Sangju city hall, Korea, he entered the Graduate School at the University of Texas at Austin in August 2000. He started working on electronic transport experiments through nanoscale devices for his Ph.D. project, supervised by Prof. Zhen Yao. He finished his Ph.D. in the summer of 2006 after spending six years in Austin. He will join von Klitzing's department in Max-Planck-Institut für Festkörperforschung in Stuttgart, Germany as a postdoctoral fellow in October, 2006.

Permanent address:
229 Bugok Kong-Gum, Sangju, Kyungbuk, Zip: 742-822
South Korea

This dissertation was typed by the author.